Journal of Sustainable Food, Water, Energy and Environment (JSFWEE)

Publisher

Faculty of Graduate Studies and Environmental Research, Sohag University, Egypt

Volume 1. Issue 2 October 2025

Print ISSN 3062-5513 Online ISSN 3062-5521

Journal of Sustainable Food, Water, Energy and Environment (JSFWEE)

(Faculty of Graduate Studies and Environmental Research, Sohag University)

The JSFWEE is a peer-reviewed specialized journal. It is published both online and in print. The journal published biannually by Faculty of Graduate Studies and Environmental Research at Sohag University which is concerned with publishing original, methodological, and plagiarism-free papers in theoretical and experimental papers of all sustainable issues of food, water, energy and environment as well as the intersection of these two fields with each other and with other fields of research. Its editorial board includes efficient and reputable professors. In addition, the manuscripts are reviewed by experienced, reputable reviewers. The JSFWEE is an opportunity for international researchers to publish original papers and materials publishes original research articles, comprehensive review articles, short communications and notes in English

Aims and scope of the journal

The Journal of sustainable food, water energy and environment (JSFWEE) is a multidisciplinary peer-reviewed international journal. JSFWEE aims to improve and disseminate knowledge on the methods, technologies and policies needed to develop and sustain food, water, energy and the environment by decoupling growth from natural resources and replacing it with a knowledge-based economy, taking into account its economic, environmental and social pillars, as well as methods for assessing and measuring the sustainability of development, in relation to food, water, energy and environment production systems and their many combinations. JSFWEE publishes theoretical and experimental papers of basic and applied research. The scope of JSFWEE includes all sustainable issues of food, water, energy and environment with a wide but in-depth coverage. JSFWEE publishes original research articles, comprehensive review articles, short communications and notes to the editor within the scope of the journal.

Objectives of the journal

1. **To publish innovative and original research that fulfill the methodologies and standards of the fields of food, water, energy and environment sustainability.**
2. **To disseminate knowledge on the methods, technologies and policies needed to develop and sustain food, water, energy and the environment by decoupling growth from natural resources and replacing.**
3. **Providing a publishing platform for researchers that links food, water, energy and environment sustainability.**

4. To feature current theories, concepts, ideas and trends in the fields of food, water energy and environment sustainability.

Publication Frequency

The JSFWEE is published biannually in March and September.

Fields of specialization

The scope of the journal includes the following specific areas:

- **All disciplines of food sustainability, Agricultural and food economics**
- **Urban agriculture**
- **Climate-smart food systems**
- **Crop biology and sustainability**
- **Agroecology and ecosystem services**
- **Nutrition and sustainable diets agro-food safety**
- **Social movements, institutions, and governance**
- **Sustainable food processing**
- **Water-smart food production.**
- **All disciplines of water sustainability**
- **Waste management in agroecosystems**
- **Ecological and human risk assessment**
- **Environmental system modelling and optimization**
- **Biodiversity conservation and ecosystems**
- **Social, economic and policy aspects of environmental management**
- **Targets, Technologies and strategies for developing the decision-making framework in the water sector**
- **Urban planning addressing water and environmental sustainability**
- **Hydrology and hydrogeology**
- **Atmospheric pollutants and trace gases, solid and hazardous waste management**
- **Probabilistic modelling of water resources**
- **Related researched on Environmental Sciences**
- **Uncertainty assessment in impact studies**
- **Energy and nutrient recovery in wastewater treatment**
- **All disciplines of energy sustainability, Renewable Energy Sources**
- **Economics of sustainable energy systems**
- **Educational and technological research papers on sustainable Energy**
- **Sustainable energy efficiency and sustainable energy conservation**
- **Photovoltaics**
- **Combined and hybrid sustainable energy systems**
- **Smart grids**
- **Carbon capture and storage**
- **Sustainability in the urban environment**
- **Energy and environmental policies**
- **Social dimensions of energy and sustainability.**
- **Concentrated Solar Technology**
- **Biomass and bioenergy**
- **Marine and hydropower energy systems**
- **Environmental chemistry and biology**

Contents

Volume 1. Issue 2, April 2025

Journal of sustainable food, water, energy and environment

Deposition parameters influencing structural and optical properties of SnO_2/TiO_2 thin films for UV photodetector environmental monitoring applications

M. A. Awad[1], Abdalrahman M. Rayan[1], S.H. Mohamed[1,2]

[1]Physics Department, Faculty of Science, Sohag University, 82524 Sohag, Egypt
[1]Falculty of Graduate Studies and Environmental Research, Sohag University, 82524 Sohag, Egypt

Received: 22 June. 2025, Revised: 8 July. 2025, Accepted: 21 July. 2025 Published online 31 July. 2025

Abstract: SnO_2 thin films were synthesized on pre-sputtered TiO_2 layers using a thermal chemical vapor deposition technique under two deposition parameters: a high oxygen flow rate (200 sccm; sample 1) and a long deposition time (180 min; sample 2). The influence of deposition parameters on the overall properties was systematically investigated using different analytical techniques. X-ray diffraction revealed high crystalline quality with three intermixed phases - SnO_2, TiO_2 and $Ti_{26.72}O_{48}$ for sample 2, in contrast to those synthesized at 200 sccm (sample 1). Morphological analysis supports the structural findings by revealing a uniform and denser microstructure in thin films prepared with moderate oxygen flow (75 sccm) but longer deposition time 180 min. Optical measurements showed moderate transparency under both conditions, with slightly lower transparency (60%), a higher refractive index (3.03) and a wider optical band gap (3.64 eV) in the thin films of sample 2. The static dielectric constant (ε_0) obtained from the theoretical Penn model and semi empirical Adachi relation showed close proximity. These findings suggest the promise of using SnO_2/TiO_2 thin films prepared under extended deposition time (180 min) to be valuable in applications such as UV photodetectors for environmental monitoring.

Keywords: SnO_2/TiO_2; long deposition parameters; high oxygen flow rate; static dielectric constant; Penn model; Adachi relation

1. Introduction

Metal oxide thin films have been extensively studied for several decades due to their numerous applications in various fields such as photodetectors [1, 2], gas sensors [3], photocatalysis [4], solar cells [5], etc. These widespread applications derived from their unique advantages, such as high optical transparency [6], good electrical conductivity [6], and high thermal stability [7]. Among these metal oxides, SnO_2 and TiO_2 are of particular interest. Where their combination in heterostructure offers a strategy to enhance their performance through combining the advantages of the two oxides. The usage of TiO_2 as a buffer substrate improves adhesion of the epitaxial layer, influences the crystal orientation, and enhances charge separation that is beneficial for applications such as UV photodetectors, photocatalysis, and gas sensors [8-10]. The performance of SnO_2/TiO_2 thin films is greatly dependent on deposition parameters, which significantly affect crystallinity, morphology, optical and electrical characteristics.

In this study, SnO_2 thin films were deposited on pre-sputtered TiO_2 layers using the thermal chemical vapor deposition technique under two different experimental conditions: a high oxygen flow rate of 200 sccm and an extended deposition time of 180 min. The aim was to compare the impact of deposition parameters on overall properties of the prepared films. The results indicated that thin films prepared at extended deposition times (180 min) exhibited superior characteristics, such as high crystalline quality, uniform and dense surface morphology, good optical, electrical, and dielectric properties. This highlights their potential usage in applications such as UV photodetectors, photocatalysis, and semitransparent electrodes in solar cells.

2. Experimental

Thin films of SnO_2/TiO_2 thin films were synthesized in two step processes using DC magnetron sputtering followed by CVD technique. Before deposition, Si and glass substrates were ultrasonically cleaned in an acetone for 15 min followed by deionized water and then they are carefully dried. In the sputtering system, the TiO_2 buffer layer was carefully grown using Ti target under oxygen (O), nitrogen (N) and argon (Ar) flow rate of 15, 60 and 25 sccm,

* Corresponding author E-mail: arwamadeha@yahoo.com Print ISSN 3062-5513 Online ISSN 3062-5521

respectively. Where these thin films were then used as substrate for the subsequent growth of SnO_2 thin films. The deposition of SnO_2 in CVD technique was under two different experimental conditions as shown in Table 1. At the end of each experiment, the furnace was left to cool naturally to room temperature while maintain the Ar flow to protect the rapid oxidation.

The thicknesses of the SnO_2/TiO_2 thin films were measured utilizing Form Talysurf 50 profilometer. The obtained values are listed in Table 1. The produced SnO_2/TiO_2 thin films were subjected to various characterization techniques to analyze their structural, morphological, optical and electrical properties. X-ray diffraction (XRD) was used to analyze the crystal structure using Bruker D8-Advanced X-ray diffractometer. The morphological and compositional analysis were conducted using scanning electron microscope (SEM) and energy dispersive analysis of X-ray (EDAX) (JEOL, Japan), respectively. The optical properties were measured in the wavelength range 200-1200 nm using spectrophotometer.

Table 1: CVD preparation conditions and thicknesses obtained from Form Talysurf 50 profilometer.

Sample	Temp. (°C)	Ar flow rate (sccm)	O_2 flow rate (sccm)	Deposition Time (min)	Thickness of SnO_2/TiO_2 (nm)
Sample 1	400	200	200	90	310/103
Sample 2	400	200	75	180	301/103

3. Results and discussions

3.1 Microstructural analysis

The XRD of SnO_2/TiO_2 thin films at an oxygen flow rate of 200 sccm (Fig. 1a) demonstrates a very low crystalline nature, where only two distinct planes of (011) and (222) associated with the TiO_2 phase (COD 5000223) [11] and the $Ti_{26.72}O_{48}$ phase (COD database code: 9014505) are observed. The absence of SnO_2 peaks although deposition suggests the amorphous distribution with no long-range structural order. In contrast, the crystal structure of SnO_2/TiO_2 deposited with 75 sccm and for 180 min (Fig. 1b) reveals the formation of a polycrystalline structure, where all diffracted peaks are predominantly related to the rutile SnO_2 phase (COD 1534785) with preferred orientation along the (200) plane. This preferred orientation indicates the anisotropic growth of SnO_2 phase that reduces charge carrier scattering and enhances the electrical and overall properties of the prepared thin films [12].

The crystallite size (D) of SnO_2/TiO_2 thin films was calculated using the Scherrer equation [13], given through

$$D = \frac{K\,\lambda}{\beta\, cos\theta} \qquad (1)$$

where λ is the x-ray wavelength equal to 1.54060 Å, β is the FWHM, θ is the Bragg angle in radians, and K is the shape factor with a value usually ~ 0.9. Based on the (222) diffraction planes at 2θ = 31.78° and FWHM of 0.12686°, the crystallite size of thin films prepared at oxygen flow rate of 200 sccm is 65.11 nm. On the other hand, for thin films deposited at 180 min (Fig. 1b), the crystallite size was calculated using the (200) diffraction planes. Where the calculated crystallite size was 48.75 nm using 2θ of 37.84° and FWHM of 0.17237°. Worth noting, crystallites size from XRD shows an apparent contradiction when compared with the crystal structure depicted in Fig. 1a and 1b. The reason is that the Scherrer equation estimates crystallite size only from a specific crystallographic plane. Moreover, it is important to clarify that higher crystallinity doesn't mean larger crystallite size, where thin films composed of numerous small, well-ordered crystallites can produce sharp and intense XRD peaks, which in turn produce relatively small crystallites size. On contrary, in Fig. 1a the presence of localized large crystallites, particularly from (222) planes, lead to large crystallites size even though the overall film crystallinity is lower.

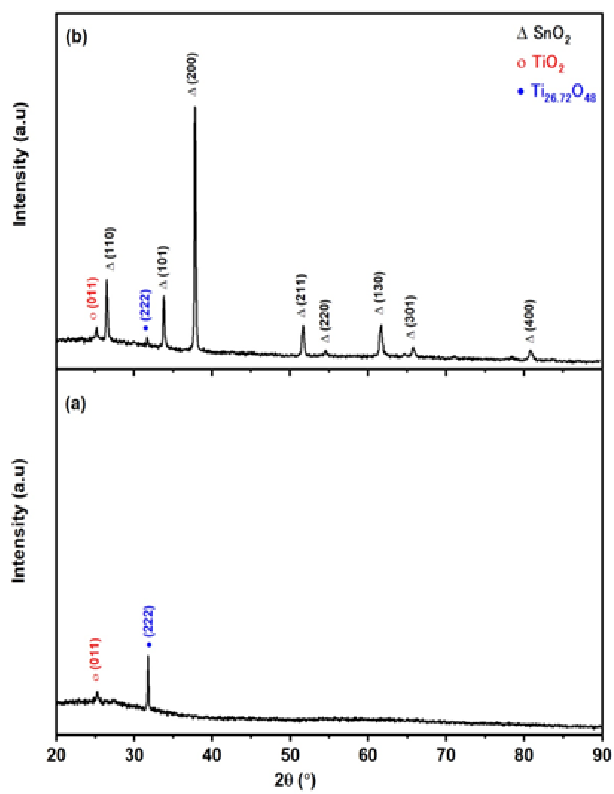

Fig. 1: The XRD of SnO_2/TiO_2 thin films at an oxygen flow rate of 200 sccm, sample 1, (a) long deposition time 180 min, sample 2, (b).

Fig. 2 compare the surface morphology analysis of SnO2/TiO2 thin films of sample 1 (Fig. 2a) and sample 2 (Fig, 2b). Clearly, randomly distributed and loosely packed nanocrystallites are observed at high oxygen flow rate (sample 1) which are not achieved at long deposition time (sample 2), where more dens and grains packing are observed. These results of surface morphology support the XRD results depicted in Fig. 1.

The EDAX spectrum of sample 1 is shown in Fig. 2c and it confirms the presence of Sn, O, and Ti peaks whereas Cl peaks originate from the residual chloride precursor. On the other hand, in Fig. 2d (sample 2), the Cl peaks are not observed due to their removal at long deposition time (180 min).

3.2 Optical and dielectric properties

The optical behavior of SnO_2/TiO_2 thin films (Fig. 3) is strongly dependent on their structural and morphological properties. Where thin film deposited at a high oxygen flow rate (Sample 1) exhibits lower than expected transparency (~ 70% in the visible to near IR region). This reduction is attributed to the poor crystallinity of the as grown thin films (Fig. 1a), that increases light scattering [14]. These structural inhomogeneities increase light scattering and surface reflectance [14], especially in the visible spectral range. On the other hand, the thin films deposited for longer deposition time (sample 2) shows relatively low transparency (~ 60%) despite the high crystal ordering. The reason relies on increasing film thickness that increased the light polarization [15].

The optical band gap was calculated using the direct allowed transition of the Tauc equation [16] (Fig. 4) given by

$$(\alpha h\nu)^2 = \beta(h\nu - E_g) \qquad (2)$$

where α is the absorption coefficient and hν is the photon energy. For SnO_2/TiO_2 deposited under a high oxygen flow rate (sample 1), the calculated E_g value was 3.58 eV. In contrast, the thin films deposited with a longer deposition time (sample 2) and a moderate oxygen flow rate (75 sccm) possess a higher optical band gap value (E_g = 3.64 eV). The improved crystallinity, which reduced the defect states and shifted the absorption to higher energies, is responsible for this increase [6].

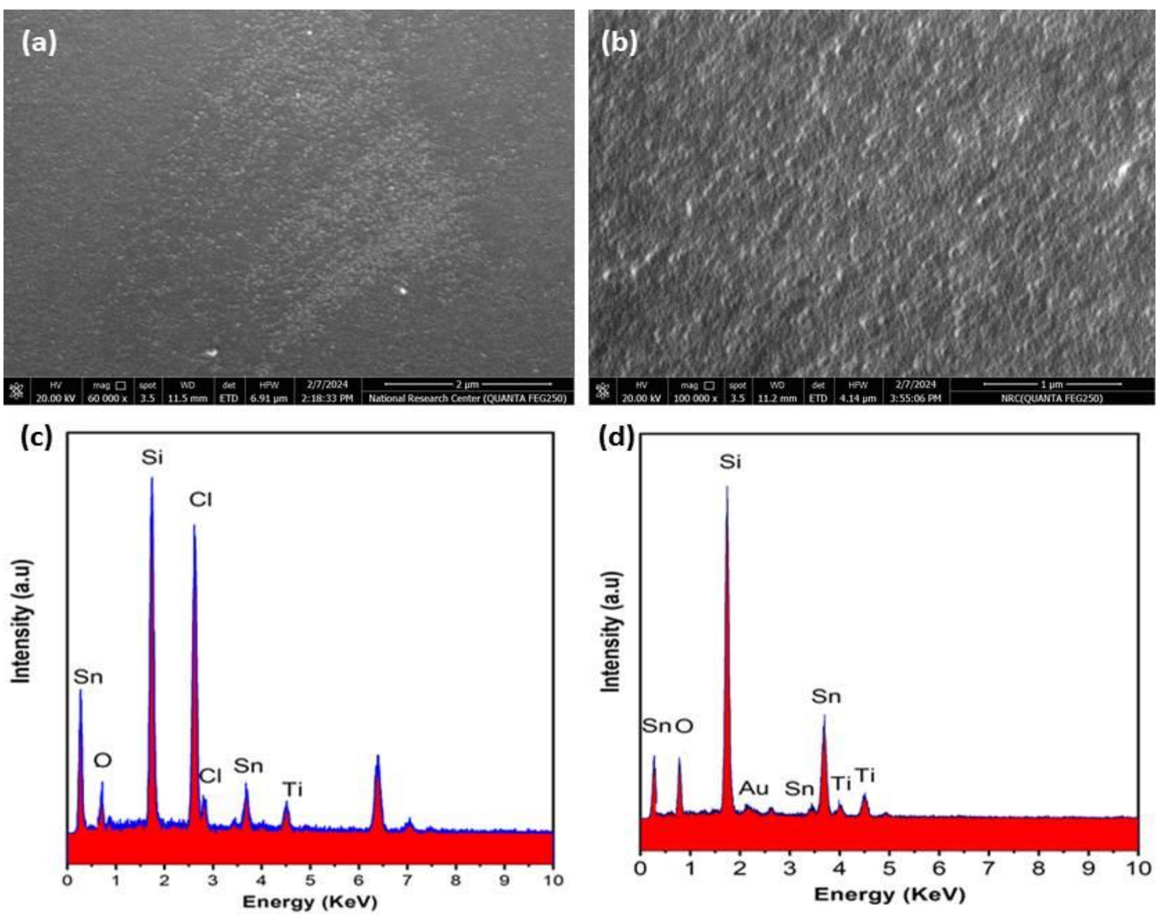

Fig. 2: SEM images of (a) sample 1 and (b) sample 2. EDAX spectra of (c) sample 1 and (d) sample 2.

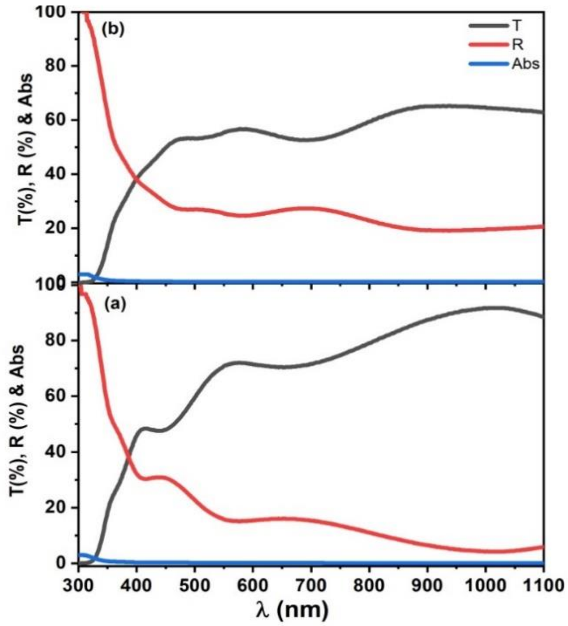

Fig**. 3:** Optical transmittance, reflectance and absorbance of (a) sample 1 and (b) sample 2.

Fig. 5 depicts the refractive index (n) and extinction coefficient (k) of SnO_2/TiO_2 thin films deposited at a high oxygen flow rate (Fig. 5a; sample 1) and at a long deposition time (Fig.5b; sample 2). The thin films deposited for a long deposition time show a higher refractive index (n = 3.03 at 600 nm) compared to those deposited at a high oxygen flow rate (2.36 at 600 nm). This increase is attributed to enhanced crystallinity and denser microstructure that increases light polarization [15]. On regard to the extinction coefficient (k), both films show high value in the UV range as a result of electron transfer from the valence band to the conduction band. As the wavelength increases, the extinction coefficient decreases for both condition (sample 1 and sample 2). The slightly high k values observed for the films with longer deposition time, especially in the NIR region, suggest increased optical losses due to the increase of free carrier absorption [17-19].

In order estimate the dielectric properties of SnO_2/TiO_2 thin films at constant electric field, the static dielectric constant ε_0 was approximated using the theoretical Penn model [20] for wide band gap semiconductors using the relation

$$\varepsilon_0 = 1 + \left(\frac{\hbar\omega_p}{E_g}\right)^2 \qquad (3)$$

where E_g is the optical band gap and ω_p is the plasma frequency and $\hbar$ is the reduced Planck constant. For many wide band gap semiconductors, the plasma energy ($\hbar\omega_p$) is typically taken as 9- 10 eV [21,22]. Using the value of 10 eV and the band gap energy of 3.58 and 3.64 eV for SnO_2/TiO_2 thin films deposited at high oxygen flow rate (sample 1) and long deposition time (sample 2), respectively, yields dielectric constant values of 8.81 and 8.55, respectively. These values reflect the strong polarizability of the prepared thin films, where their values are higher than that was reported for single phase of SnO_2.

The static dielectric constant of SnO_2/TiO_2 thin films is also calculated using semi-empirical Adachi relation [22] given through,

$$\mathcal{E}_0 = 18.52 - 3.08\ E_g \qquad (4)$$

yielding values of 7.49 and 7.31 for thin films prepared at high oxygen flow rate (sample 1) and long deposition time (sample 2).

Comparing the static dielectric constant calculated using Penn model and Adachi relation shows close agreement and are consistent with the values reported in the literature [6,24].

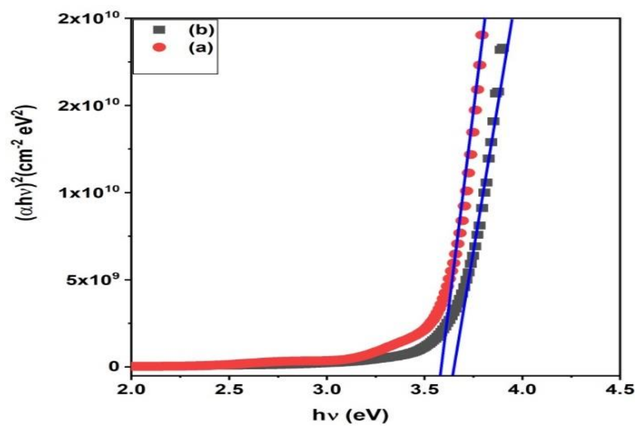

Fig. 4: $(\alpha h\nu)^2$ versus $h\nu$ plots.

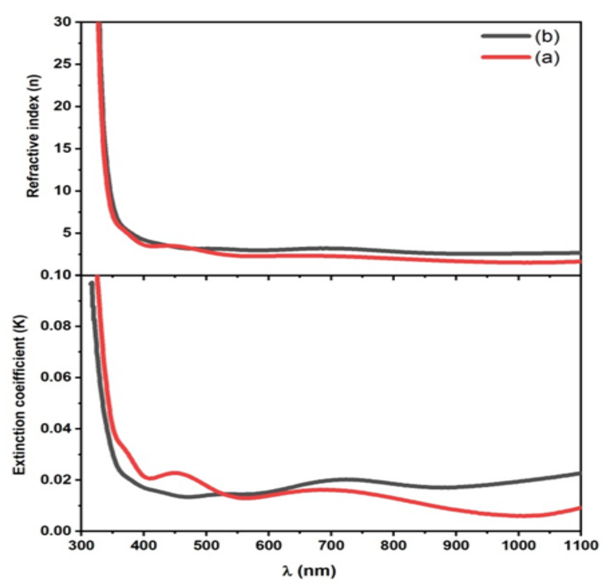

Fig. 5: refractive index and extinction coefficient of (a) sample 1 and (b) sample 2.

4. Conclusion

SnO_2 thin films is successfully deposited on TiO_2 thin films using CVD technique under two different conditions of high oxygen flow rate (sample 1) and long deposition time (sample 2), while maintaining constant furnace temperature and Ar flow rate. High crystalline quality and compacted uniform microstructure were obtained for thin film prepared at long deposition time which is not achieved at high oxygen flow rate. The static dielectric constant estimated via both the Adachi and the Penn model showed close agreement. These finding suggests the possibility of using SnO_2/TiO_2 thin films prepared at long deposition time in applications such as UV photodetector environmental monitoring.

5. References

[1] T. Zhai, X. Fang, M. Liao, X. Xu, H. Zeng, B. Yoshio, D.J.S. Golberg, A comprehensive review of one-dimensional metal-oxide nanostructure photodetectors, Sensors vol. 9, pp. 6504-6529, 2009.

[2] M. A. Awad, M. Shaban, M. Rabia, The efficiency of M (M= Li, Na, or Cs) doped CdS nanomaterials in optoelectronic applications, Int. J. Energy Res. Vol. 46 pp. 8443-8451, 2022.

[3] Y. Yoon, P. L. Truong, D. Lee, S. H. Ko, Metal-oxide nanomaterials synthesis and applications in flexible and wearable sensors, ACS Nanosci. Au vol. 2, 64−92, 2022.

[4] D. Nunes, A. Pimentel, R. Branquinho, E. Fortunato, R.J.C. Martins, Metal oxide-based photocatalytic paper: A green alternative for environmental remediation, Catalysts vol. 11, pp. 504, 2021.

[5] H. Soonmin, A review of metal oxide thin films in solar cell applications, Int. J. Thin Films Sci. Technol. vol. 11, pp. 37-45, 2022.

[6] M. A. Awad, E.R. Abaza, E.R. Shaaban, Optimizing the conditions to synthesize transparent conductive SnO_2 thin films for optoelectronic applications, Surf. Interfaces vol. 69, pp. 106734, 2025.

[7] M. A. Awad, E. M. M. Ibrahim, A, M. Ahmed, Synthesis and thermal stability of ZnO nanowires, J. Therm. Anal. Calorim. Vol. 117, pp. 635-642, 2014.

[8] K. Maver, I. Arčon, M. Fanetti, S. Al Jitan, G. Palmisano, M. Valant, U.L. Štangar, Improved photocatalytic activity of SnO_2-TiO_2 nanocomposite thin films prepared by low-temperature sol-gel method, Catal. Today vol. 397-399, pp. 540-549, 2022.

[9] M.J. Jeong, S.W. Lee, Y. Shin, J.-H. Choi, J.-H.J.S. Ahn, Implementation of rutile-TiO_2 thin films on TiN without post-annealing through introduction of SnO_2 and its improved electrical properties, Surf. Interfaces vol. 42, pp. 103420, 2023.

[10] B. Yadav, N. Verma, S.J.O. Singh, L. Technology, Nanocrystalline SnO_2–TiO_2 thin film deposited on base of equilateral prism as an opto-electronic humidity sensor, Opt. Laser Technol. vol. 44, pp. 1681-1688, 2012.

[11] S. Sönmezoğlu, A. Arslan, T. Serin, N. Serin, The effects of film thickness on the optical properties of TiO_2–SnO_2 compound thin films, Physica Scripta vol. 84, pp. 065602, 2011.

[12] V. Consonni, G. Rey, H. Roussel, B. Doisneau, E. Blanquet, D.J. Bellet, Preferential orientation of fluorine-doped SnO_2 thin films: The effects of growth temperature, Acta Mater. vol. 61, pp. 22-31, 2013.

[13] A. Monshi, M.R. Foroughi, M.R. Monshi, engineering, Modified Scherrer equation to estimate more accurately nano-crystallite size using XRD, World J. Nano Sci. Eng. vol. 2, pp. 154-160, 2012.

[14] M. A. Awad, M.J.A.P.A. Rabia, Optimal temperature and Mn content for enhancing optical properties and inducing room temperature ferromagnetism of Mn doped In_2O_3 nanocubes, Appl. Phys. A vol. 128, pp. 225, 2022.

[15] M. A. Awad, M. Rabia, The bimetallic synthesis of TeO_2–Sb_2O_4 thin films for optoelectronic applications, Ceram. Int. vol. 49, pp. 37340-37348, 2023.

[16] Ł. Haryński, A. Olejnik, K. Grochowska, K.J. Siuzdak, A facile method for Tauc exponent and corresponding electronic transitions determination in semiconductors directly from UV–Vis spectroscopy data, Opt. Mater. vol. 127, pp. 112205, 2022.

[17] M. A. Awad, A. H. Aly, Experimental and theoretical studies of hybrid multifunctional TiO_2/TiN/TiO_2, Ceram. Int. vol. 45, pp. 19036-19043, 2019.

[18] S.H. Mohamed, K.M. Al-Mokhtar, Characterization of Cu_2O/CuO nanowire arrays synthesized by thermal method at various temperatures, Appl. Phys. A vol. 124, pp. 493, 2018.

[19] H. A. Mohamed, H. M. Ali, S. H. Mohamed and M. M. Abd El-Raheem, Transparent conducting ZnO-CdO thin films deposited by e-beam evaporation technique, Eur. Phys. J. Appl. Phys. vol. 34, pp. 7-12, 2006.

[20] A.J. Sharma, Size-dependent energy band gap and dielectric constant within the generalized Penn model applied to a semiconductor nanocrystallite, J. Appl. Phys. vol. 100, pp. 084301, 2006.

[21] R. Ravichandran, A.X. Wang, J.F. Wager, Solid state dielectric screening versus band gap trends and implications, Opt. Mater. vol. 60, pp. 181-187, 2016.

[22] N. Ravindra, P. Ganapathy, J.J. Choi, Energy gap–

refractive index relations in semiconductors–An overview, Infrared Phys. Technol. vol. 50 pp. 21-29, 2007.

[23] S. Adachi, Properties of semiconductor alloys: group-IV, III-V and II-VI semiconductors, John Wiley & Sons 2009.

[24] M.A. Yıldırım, The effect of copper concentration on structural, optical and dielectric properties of $Cu_xZn_{1-x}S$ thin films, Opt. Commun. vol. 285, pp. 1215-1220, 2012.

Journal of sustainable food, water, energy and environment

The applications of X-ray technology in medical imaging: advances, challenges, and future perspectives (A review)

*Abdalrahman M. Rayan[1,] *, Ahmed Adam[2], Gehad Al-Arabi[3], and Mahrous R. Ahmed[1]*

[1]Physics Department, Faculty of Science, Sohag University, Sohag 82524, Egypt

[3]Botany and microbiology Department, Faculty of Science, Sohag University, Sohag 82524, Egypt

[2]Urology Department, Faculty of Medicine, Sohag University, Sohag 82524, Egypt

Received: 11 June. 2025, Revised: 24 Aug. 2025, Accepted: 25 Aug. 2025 Published online 24 Sep. 2025

Abstract: In 1895, Wilhelm Conrad Röntgen (1845–1923) pioneered X-ray imaging, which revolutionized medical diagnosis and modern healthcare. X-ray imaging's fundamentals, therapeutic uses, technology advances, and future directions are examined in detail. X-rays contrast bone and soft tissues by attenuation, absorption, and scattering. X-ray medical usage. In diagnostic radiography, it is best for fracture diagnosis, chest pathology, including pneumonia, lung cancer, and dental checks. Angiography, catheter insertion, and GI (gastrointestinal issues) diagnostics benefit from real-time dynamic fluoroscopy. Early breast cancer detection is improved by mammography, especially DBT (Digital breast tomosynthesis). Cross-sectional X-ray imaging using multi-slice contrast-enhanced CT (Computed Tomography). Fast, inexpensive, non-invasive, good spatial resolution for osseous structures, and widely available in healthcare, X-ray imaging. These benefits are negated by ionizing radiation dangers (requiring rigorous ALARA (As Low as Reasonably Achievable) standards), worse soft-tissue contrast compared to MRI (magnetic resonance imaging) or ultrasound, limited 3D visualization without CT, and technical challenges in obese or anatomically complex patients. Technological advances alter X-rays. Digital radiography has enhanced image quality, workflow efficiency, and fracture and pneumonia screening accuracy using AI. Low-dose imaging, especially in kids, and portable critical care point-of-care technology advances. Photon-counting CT, phase-contrast imaging, and dark-field X-rays will depict soft tissues like never before, while AI (Artificial Intelligence) will speed up and improve diagnosis. Reduced doses optimize X-ray risk-benefit ratios. X-rays' efficiency, accessibility, and diagnostic ability make them crucial in medicine, even as other imaging technologies emerge. This study emphasizes the necessity for ongoing innovation to overcome limitations and preserve precision medicine benefits. X-ray imaging will remain vital to medical diagnostics with improved technology and safety precautions.

Keywords: X-ray imaging; radiography; computed tomography; medical diagnostics; radiation safety; and artificial intelligence

Abbreviations:

- GI gastrointestinal issues
- DBT (Digital breast tomosynthesis)
- CT (Computed Tomography)
- ALARA As Low as Reasonably Achievable
- MRI magnetic resonance imaging
- AI Artificial intelligence
- kVp kilovolt age peaks
- TB tuberculosis
- CAD computer-aided detection
- CCD Charge-Coupled Device
- CMOS Complementary Metal-Oxide-Semiconductor
- CBCT Cone-beam computed tomography
- ANB (Angle of point A, Nasion, and point B)
- ABC Automatic Brightness Control
- fps frames per second
- CVC Central venous catheter
- LIH last-image-hold
- SFM screen-film mammography
- FFDM full-field digital mammography
- mGy Mille gray
- DMIST Digital Mammographic Imaging Screening Trial
- ACR The American College of Radiology
- DBT Digital Breast Tomosynthesis
- CDR cancer detection rates
- C-View™ is a Hologic software that generates synthesized 2D images from 3D mammography data, specifically tomosynthesis scans
- CEM Contrast-enhanced mammography
- PCDs Photon-counting detectors
- MSCT Multi-Slice Computed Tomography
- CECT contrast-enhanced Computed Tomography

* Corresponding author E-mail: muhmedabdalrahman912@gmail.com Print ISSN 3062-5513 Online ISSN 3062-5521

- MPR Multiplanar reconstructions
- MIP maximum intensity projections
- RECISTResponse Evaluation Criteria in Solid Tumors
- DECT Dual-energy Computed Tomography
- The TNM classification It's a classification is a globally recognized system for classifying the extent of cancer spread in solid tumors. It stands for Tumor, Node, and Metastasis
- The ASPECTS Alberta Stroke Program Early CT Score) is a 10-point scoring system used to assess the extent of early ischemic changes in the brain, particularly in patients with suspected acute ischemic stroke
- IR Iterative reconstruction
- DR digital radiography
- PACS Picture archiving and communication systems
- The LNT The linear no-threshold
- BEIR VII report refers to Health Risks from Exposure to Low Levels of Ionizing Radiation
- DQE quantum detection efficiency
- AUC achieving area-under-the-curve
- CADx computer-aided diagnosis
- MBIR model-based iterative reconstruction
- VAP ventilator-associated pneumonia
- AEC automatic exposure control
- Wireless DICOM transmission the process of sending and receiving medical images and related data, adhering to the Digital Imaging and Communications in Medicine (DICOM) standard, over a wireless network
- CNNs convolutional neural networks
- NLP Natural language processing
- PACS in picture archiving and communication systems
- EID energy-integrating detector
- PCI phase-contrast imaging
- DFI dark-field imaging

1. Introduction

The discovery of X-rays in 1895 by Wilhelm Conrad Röntgen marked a revolutionary milestone in both physics and medicine [1-4]. While experimenting with cathode rays in his laboratory at the University of Würzburg, Röntgen observed an unexpected phenomenon: a fluorescent screen in his lab glowed despite being shielded from visible light. He deduced that an invisible, highly penetrating form of radiation was responsible, termed “X-rays” (X for unknown) [5]. His systematic experiments, including the iconic image of his wife Anna Bertha's hand, revealing bones and her wedding ring, demonstrated the technology's potential to visualize internal structures non-invasively.

By 1896, X-rays were already being used clinically to locate fractures and foreign objects, earning Röntgen the first Nobel Prize in Physics (1901) [4, 6]. The rapid adoption of X-rays transformed medical diagnostics [7-9], replacing invasive methods and guesswork with precise anatomical imaging. Over time, advancements such as digital radiography [10-13], computed tomography (CT) [14-17] and fluoroscopy [18-20] expanded their applications from detecting tuberculosis to guiding surgical procedures. However, early use also revealed risks, including radiation burns and cancer [21-24], leading to the development of safety protocols (e.g., ALARA principle) [25-28]. Today, X-rays remain indispensable in emergency medicine, oncology, and dentistry, while ongoing innovations—like AI-assisted interpretation and low-dose techniques—address their limitations [29-31]. As we reflect on Röntgen's legacy, X-ray imaging continues to evolve, balancing diagnostic power with patient safety in modern healthcare.

X-rays remain a cornerstone of modern medical diagnostics due to their unparalleled ability to non-invasively visualize internal anatomical structures with high resolution and rapid acquisition. Since its discovery in 1895, X-ray imaging has become indispensable across multiple medical specialties, including radiology, orthopedics [32-34], pulmonology [35-37], dentistry [38-40], and emergency medicine [41, 42]. Their primary utility lies in the detection of fractures, dislocations, and degenerative bone diseases, where their high spatial resolution allows for the precise assessment of skeletal integrity. In chest radiography, X-rays serve as a first-line diagnostic tool for identifying pulmonary pathologies such as pneumonia [43, 44], tuberculosis [45-47], pleural effusions [48-50], and malignancies [51], often guiding further investigations like CT or biopsy. Additionally, dental radiography is critical for diagnosing caries, periodontal disease, and impacted teeth, while mammography plays a vital role, significantly improving patient outcomes through early intervention [52-56]. Beyond static imaging, fluoroscopy enables real-time dynamic assessment, facilitating complex procedures such as angiography, catheter placements, and gastrointestinal studies [20, 57, 58]. Despite the advent of advanced modalities like MRI [59, 60] and ultrasound [61, 62], X-rays retain widespread use due to their cost-effectiveness, accessibility, and rapid turnaround time, making them particularly valuable in emergency and resource-limited settings. However, the ionizing nature of X-rays necessitates strict adherence to radiation safety protocols to minimize patient and occupational exposure risks [63, 64]. Ongoing advancements, including digital radiography, AI-assisted image analysis, and low-dose techniques, continue to enhance diagnostic accuracy while mitigating radiation hazards. Thus, X-rays remain an irreplaceable tool in modern medicine, balancing diagnostic efficacy, efficiency, and safety in clinical practice.

Figure 1: Anna Bertha's hand, where the wedding ring appears in her hand [1]

By 1896, X-rays were already being used clinically to locate fractures and foreign objects, earning Röntgen the first Nobel Prize in Physics (1901) [4, 6]. The rapid adoption of X-rays transformed medical diagnostics [7-9], replacing invasive methods and guesswork with precise anatomical imaging. Over time, advancements such as digital radiography [10-13], computed tomography (CT) [14-17] and fluoroscopy [18-20] expanded their applications from detecting tuberculosis to guiding surgical procedures. However, early use also revealed risks, including radiation burns and cancer [21-24], leading to the development of safety protocols (e.g., ALARA principle) [25-28]. Today, X-rays remain indispensable in emergency medicine, oncology, and dentistry, while ongoing innovations—like AI-assisted interpretation and low-dose techniques—address their limitations [29-31]. As we reflect on Röntgen's legacy, X-ray imaging continues to evolve, balancing diagnostic power with patient safety in modern healthcare.

X-rays remain a cornerstone of modern medical diagnostics due to their unparalleled ability to non-invasively visualize internal anatomical structures with high resolution and rapid acquisition. Since its discovery in 1895, X-ray imaging has become indispensable across multiple medical specialties, including radiology, orthopedics [32-34], pulmonology [35-37], dentistry [38-40], and emergency medicine [41, 42]. Their primary utility lies in the detection of fractures, dislocations, and degenerative bone diseases, where their high spatial resolution allows for the precise assessment of skeletal integrity. In chest radiography, X-rays serve as a first-line diagnostic tool for identifying pulmonary pathologies such as pneumonia [43, 44], tuberculosis [45-47], pleural effusions [48-50], and malignancies [51], often guiding further investigations like CT or biopsy. Additionally, dental radiography is critical for diagnosing caries, periodontal disease, and impacted teeth, while mammography plays a vital role, significantly improving patient outcomes through early intervention [52-56]. Beyond static imaging, fluoroscopy enables real-time dynamic assessment, facilitating complex procedures such as angiography, catheter placements, and gastrointestinal studies [20, 57, 58]. Despite the advent of advanced modalities like MRI [59, 60] and ultrasound [61, 62], X-rays retain widespread use due to their cost-effectiveness, accessibility, and rapid turnaround time, making them particularly valuable in emergency and resource-limited settings. However, the ionizing nature of X-rays necessitates strict adherence to radiation safety protocols to minimize patient and occupational exposure risks [63, 64]. Ongoing advancements, including digital radiography, AI-assisted image analysis, and low-dose techniques, continue to enhance diagnostic accuracy while mitigating radiation hazards. Thus, X-rays remain an irreplaceable tool in modern medicine, balancing diagnostic efficacy, efficiency, and safety in clinical practice.

This review aims to provide a comprehensive analysis of the applications, benefits, limitations, and emerging trends in X-ray-based medical imaging, synthesizing current knowledge to inform clinical practice and future research. First, it examines the diagnostic and therapeutic applications of X-ray technology, including its pivotal role in radiography, fluoroscopy, computed tomography (CT), and interventional procedures. By evaluating these applications, the review highlights how X-rays facilitate rapid and accurate diagnoses in trauma, pulmonary diseases, dental disorders, and oncological imaging. Second, the discussion focuses on the advantages of X-ray imaging, such as its cost-effectiveness, widespread availability, and real-time imaging capabilities, which make it indispensable in emergency and primary care settings. However, the review also critically addresses the limitations of X-ray technology, particularly its reliance on ionizing radiation, which poses inherent risks of carcinogenesis and necessitates stringent radiation protection measures. Additionally, challenges such as limited soft-tissue contrast and overlapping anatomical structures are analysed in comparison to alternative modalities like MRI and ultrasound. Finally, the review explores future trends aimed at overcoming these limitations, including advancements in low-dose imaging techniques, artificial intelligence (AI)-enhanced diagnostics, and next-generation technologies such as phase-contrast and photon-counting CT. By integrating recent research and technological developments, this review seeks to provide a balanced perspective on the evolving role of X-rays in modern medicine, ultimately contributing to evidence-based decision-making for clinicians, researchers, and policymakers. Through this analysis, the review underscores the need for continued innovation to optimize diagnostic accuracy while minimizing risks, ensuring that X-ray technology remains both effective and safe in an era of precision medicine.

2. Discussion

2.1. Principles of X-Ray Imaging

X-rays are produced through the rapid deceleration of high-energy electrons (bremsstrahlung radiation) or electron transitions within inner atomic shells (characteristic radiation), typically within an X-ray tube. When a high-voltage potential is applied between the cathode and anode, thermionically emitted electrons are accelerated toward a tungsten target, where their sudden deceleration converts kinetic energy into X-ray photons [65, 66]. The resulting X-ray spectrum consists of a continuous bremsstrahlung spectrum superimposed with discrete characteristic peaks, dependent on the anode material and tube voltage [67, 68].

As X-rays traverse biological tissues, their interaction occurs primarily through photoelectric absorption and Compton scattering [70, 71], with relative probabilities dictated by photon energy and tissue atomic number. Photoelectric absorption, dominant at lower energies (<30 keV) and in high-Z materials like bone, results in complete photon attenuation and contributes to high-contrast imaging. In contrast, Compton scattering, prevalent at higher energies and in soft tissues, involves partial energy transfer to outer-shell electrons, generating scattered radiation that degrades image quality. A minor contribution from coherent (Rayleigh) scattering also occurs, though it does not deposit energy in tissues [72]. The differential attenuation of X-rays across tissues, owing to variations in density and atomic composition, forms the basis of radiographic contrast, enabling the visualization of anatomical structures. Modern imaging systems optimize these interactions through techniques such as beam filtration, grid use for scatter reduction, and energy-selective detection [73]. Understanding these fundamental principles is critical for optimizing diagnostic image quality while minimizing patient radiation exposure in clinical practice. Here, we will discuss the three main processes that happen during X-ray imaging. The major process is the Attenuation. It is the overarching term for the overall reduction in the intensity of the X-ray beam. When X-ray photons travel through matter (like human tissue), some of them are stopped or deflected, and the beam becomes weaker. Attenuation is not a single process; rather, it is the combined result of two phenomena, which are absorption and scattering. The attenuation process depends on the photon energy, material density, and atomic number (Z) of the absorbing medium. Attenuation determines radiographic contrast, as differential attenuation between tissues (e.g., bone vs. muscle) creates the image [74-76]. Now, interpreting the two processes which involved in attenuation:

I.Absorption (photoelectric effect) occurs when an X-ray photon transfers all its energy to an inner-shell electron, ejecting it (creating a photoelectron) and leaving a vacancy filled via characteristic radiation or Auger electrons [77, 78]. This process dominates at lower energies (<30 keV) and in High-Z materials (e.g., bone, iodine), contributing to high-contrast imaging but increasing patient dose.

II. Scattering involves partial energy transfer to the medium. Two key types are:

1.Compton scattering: The X-ray photon deflects off an outer-shell electron, losing some energy and changing direction. This dominates at higher energies (>60 keV) and in low-Z tissues (e.g., soft tissue), degrading image quality by producing scatter noise [79-82].

2.Coherent (Rayleigh) scattering: The photon is elastically scattered without energy loss, minimally affecting imaging [83, 84].

Radiographic contrast arises from differential X-ray attenuation between adjacent tissues, primarily governed by variations in tissue density, atomic number (Z), and thickness. This contrast mechanism enables the visualization of anatomical structures, with bone and soft tissue representing two extremes of radiographic differentiation.

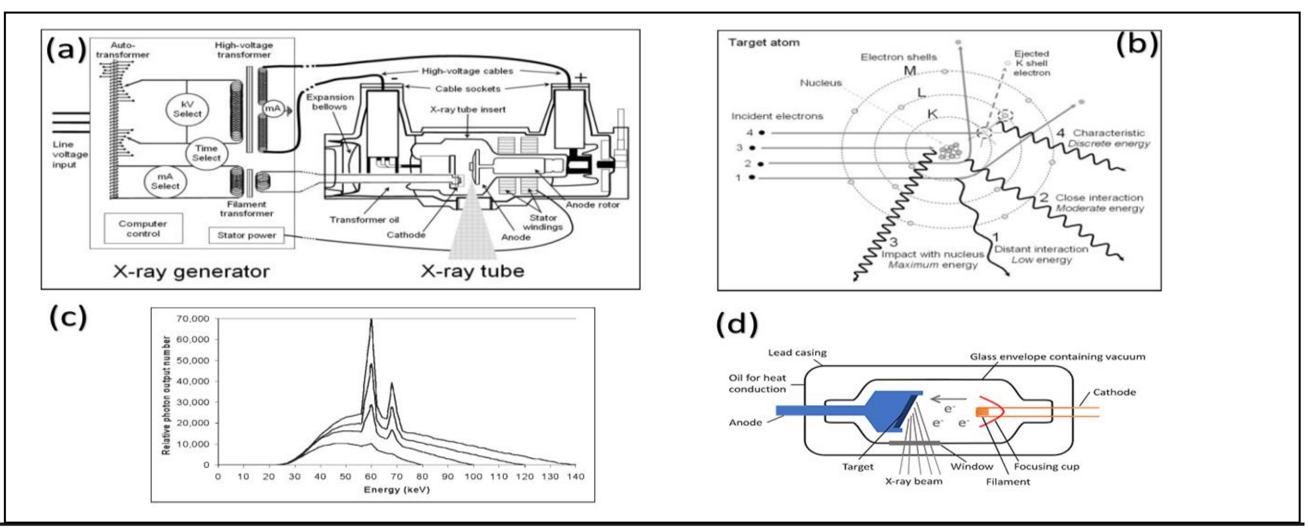

Fig. 2: The production of X-rays. (a) This figure investigates the schematic setup of the apparatus used to generate X-rays. (b) describes the atomic interaction of X-rays with the inner shells of the heavy metal atom, where it's obvious that when the electrons hit the deeper shells, high-energy X-rays are produced. (c) The X-ray spectrum is a relation between the intensity and the applied energy between the cathode and the anode. The sharp peaks that illustrate the intrinsic wavelength used in imaging or diffraction techniques. (d) a portrayal of the X-ray tube. Figures (a), (b), and (c) are taken from the reference [69]. Image (d) has been taken from the radiology café website.

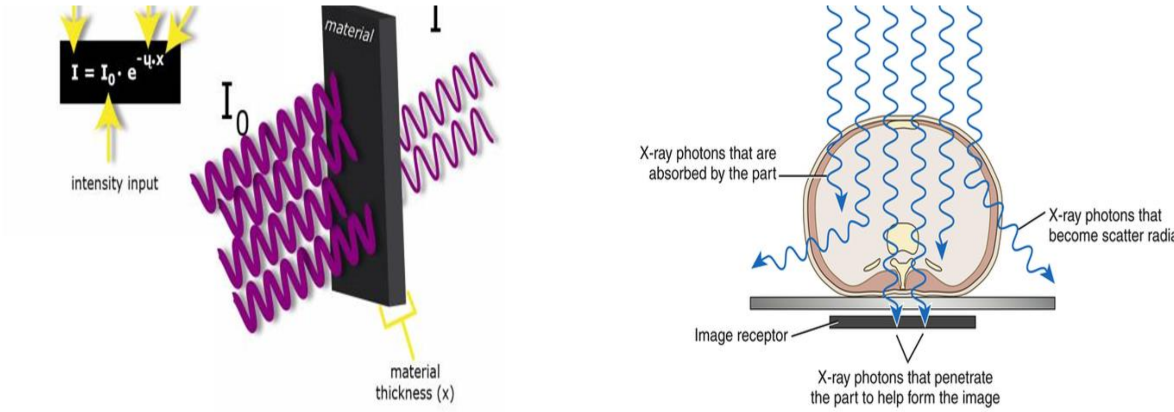

Fig. 3: (a) The attenuation process in X-ray imaging, and (b) Absorption and scattering during imaging.

2.2. Bone Imaging

Bone exhibits high radiographic contrast due to its elevated effective atomic number (Z~13) from calcium (Z=20) and phosphorus (Z=15) and greater physical density (~1.9 g/cm³). These properties enhance photoelectric absorption, particularly at lower kilovolt age peaks (kVp, typically 50-70 kVp for extremities). The significant attenuation difference between bone and surrounding soft tissues produces high-contrast images ideal for:

- Fracture detection [85, 86].
- Joint space evaluation [87].
- Skeletal abnormality assessment [88, 89].

2.3. Soft Tissue Imaging

Soft tissues (muscle, fat, organs) demonstrate lower inherent contrast due to [90, 91]:

•Similar effective Z (~7.4) and density (~1.0 g/cm³) among different soft tissues

•Compton scattering dominance at diagnostic energy ranges

•Minimal photoelectric absorption differences

Fig. 4: (a) Fracture detection. (b) Joint space evaluation, and (c) Skeletal abnormality assessment

Specialized techniques enhance soft tissue visualization:

•Mammography: Uses low kVp (25-35) to maximize photoelectric differences between fibro- glandular (Z~7.4) and adipose (Z~6.3) tissues [52, 92].

•Dual-energy subtraction: Exploits Z-dependent attenuation at different energies to separate overlapping structures [93, 94].

•Contrast agents: Introduce high-Z elements (e.g., iodine, barium) to create artificial contrast in angiography or gastrointestinal studies [95, 96].

Technical Considerations:

- kVp selection: Lower kVp increases photoelectric effect, enhancing bone contrast but increasing dose
- Scatter reduction: Grids or air gaps improve contrast by removing Compton-scattered photons
- Detector dynamic range: Modern digital systems can display both high-contrast (bone) and low-contrast (soft tissue) features simultaneously

The fundamental trade-off between contrast and radiation dose continues to drive technological advancements, including phase-contrast imaging and photon-counting detectors that promise improved soft tissue differentiation while maintaining bone visualization capabilities.

3. Clinical Applications of X-ray Imaging

3.1. Diagnostic Radiography in Fracture Detection

Diagnostic radiography remains the gold standard for fracture detection due to its ability to provide high-resolution anatomical images of bones and joints with rapid acquisition times [97]. The physical basis for fracture visualization lies in the differential attenuation of X-rays by bone tissue, which contains calcium phosphate (effective atomic number, Z~13.8) and exhibits significantly greater photoelectric absorption compared to surrounding soft tissues (Z~7.4). Standard protocols typically employ kilovoltage peaks (kVp) between 50-70 for extremities and 70-90 for larger joints, optimizing the trade-off between contrast resolution and radiation dose. At least two orthogonal projections (anteroposterior and lateral) are acquired to enable three-dimensional localization of fracture lines, with additional oblique or specialized views (e.g., Mortise view for ankle fractures) employed when clinically indicated.

Modern digital radiography systems have enhanced fracture detection sensitivity through advanced post-processing algorithms that allow simultaneous optimization of contrast and spatial resolution. Features such as edge enhancement [98] and dynamic range compression improve visualization of subtle fracture lines [99], trabecular disruptions [100], and cortical step-offs [101]. The modality demonstrates particular efficacy in detecting complete fractures (evident as radiolucent lines with irregular margins), comminated fractures (characterized by multiple bone fragments), and impacted fractures (showing areas of increased density). However, challenges persist in identifying occult fractures, especially in osteoporotic bone or anatomically complex regions like the scaphoid or femoral neck, where additional imaging with computed tomography or magnetic resonance imaging may be required.

The clinical utility of radiographic fracture assessment extends beyond initial diagnosis to include the evaluation of fracture alignment, healing progression, and potential complications such as malunion or osteomyelitis [102]. Recent advancements, including artificial intelligence-assisted fracture detection systems, have demonstrated promising results in improving diagnostic accuracy, particularly for inexperienced readers. Nevertheless, the fundamental principles of radiographic interpretation, understanding normal anatomy, recognizing fracture patterns, and correlating imaging findings with clinical presentation remain essential for optimal patient management in musculoskeletal trauma [103].

3.2. Chest X-rays in Pulmonary Pathologies (Pneumonia, Tuberculosis, Lung Cancer)

Chest radiography remains a fundamental diagnostic tool for evaluating pulmonary pathologies [104], including pneumonia [105, 106], tuberculosis (TB) [107], and lung cancer [108, 109], owing to its accessibility, cost-effectiveness, and rapid acquisition time. The inherent contrast between air-filled lungs (low attenuation) and pathological consolidations or masses (higher attenuation) enables the detection of key radiographic signs.

In pneumonia, chest X-rays reveal lobar or segmental consolidations with air Broncho-grams, typically appearing as homogenous opacities in bacterial infections, while interstitial patterns suggest viral or atypical pathogens. Tuberculosis manifests with diverse radiographic features: primary TB often presents with hilar lymphadenopathy and pleural effusions, whereas post-primary (reactivation) TB demonstrates apical cavitations, fibro nodular infiltrates, and miliary patterns in disseminated cases. For lung cancer, chest radiographs may detect solitary pulmonary nodules (>1 cm), hilar masses, or peripheral lesions with spiculated margins, though sensitivity is limited for small (<1 cm) or centrally located tumours [110, 111].

Despite its utility, chest radiography has limitations, including reduced sensitivity for early-stage malignancies and ground-glass opacities, often necessitating confirmatory CT imaging [113, 114]. Advances such as dual-energy subtraction and computer-aided detection (CAD) systems have improved diagnostic accuracy [115, 116], particularly in TB-endemic regions and lung cancer screening. Nevertheless, chest X-rays remain indispensable for initial evaluation, treatment monitoring, and follow-up of pulmonary diseases, balancing diagnostic efficacy with minimal radiation exposure.

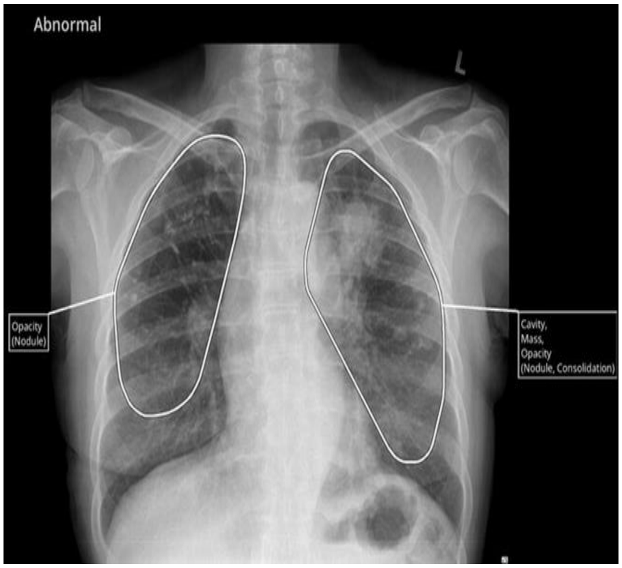

Fig. 5: An example of a chest radiograph of a patient with lung cancer [112].

3.3. Dental Radiography in Caries Detection and Orthodontic Management

Dental radiography serves as an essential diagnostic tool in modern dentistry [117, 118], enabling the detection of caries (tooth decay) and facilitating comprehensive orthodontic assessment through high-resolution imaging of dental and maxillofacial structures. The modality leverages differential X-ray attenuation between enamel (high mineral content, Z=13-15), dentin (intermediate attenuation), and carious lesions (reduced density), producing detailed images of tooth morphology and pathology [119, 120].

3.3.1 Caries Detection

Intraoral radiographs, particularly bitewing and periapical views, are the gold standard for identifying interproximal and occlusal caries that may evade visual examination. Early caries appears as radiolucent zones in enamel or dentin, while advanced lesions extend toward the pulp chamber. Digital radiography (using CCD (Charge-Coupled Device) / CMOS (Complementary Metal-Oxide-Semiconductor) sensors) enhances detection sensitivity through image enhancement algorithms, reducing radiation exposure by 50-80% compared to conventional film. Cone-beam computed tomography (CBCT) may be employed for complex cases, providing a 3D evaluation of caries extent and proximity to vital structures.

3.3.2 Orthodontic Applications

Dental radiographs play a pivotal role in orthodontic diagnosis and treatment planning:

1.Panoramic radiography assesses overall dentition, eruption patterns, and jaw relationships [121].

2.Cephalometric radiography quantifies skeletal-dental relationships (e.g., ANB (Angle of point A, Nasion, and point B) angle for malocclusion classification. [122].

3.Periapical/occlusal views evaluate root alignment and bone support prior to brace placement [123].

Emerging technologies like AI-assisted caries detection and low-dose CBCT are refining diagnostic precision while minimizing radiation risks. Nevertheless, the ALARA principle remains critical, particularly for paediatric patients requiring longitudinal monitoring.

4.Fluoroscopy: Principles and Clinical Applications in Real-Time Imaging

Fluoroscopy represents a dynamic radiographic imaging modality that enables real-time visualization of internal structures, making it indispensable for gastrointestinal (GI) studies, angiography, and catheter-guided interventions [124]. Unlike conventional radiography, which captures static images, fluoroscopy employs a continuous or pulsed X-ray beam coupled with an image intensifier or digital detector system to produce live, high-temporal-resolution imaging. This technology operates on the same fundamental principles of X-ray attenuation as standard radiography but incorporates advanced features such as automatic brightness control (ABC) and pulse-rate modulation to optimize image quality while managing radiation dose [20, 125, 126].

4.1 Gastrointestinal Studies

Fluoroscopic evaluation of the GI tract, including barium swallows, upper GI series, and small bowel follow-throughs, relies on the administration of radiopaque contrast agents (e.g., barium sulphate or water-soluble iodinated compounds) to delineate mucosal surfaces and luminal patency. Real-time imaging captures functional dynamics, such as esophageal motility disorders (e.g., achalasia), gastric emptying delays, or intestinal obstructions, with a typical frame rate of 3–30 frames per second (fps). Double-contrast techniques, combining barium and air, enhance sensitivity for detecting mucosal lesions (e.g., ulcers or early-stage neoplasms). The integration of digital subtraction fluoroscopy further improves lesion conspicuity by eliminating overlapping bone shadows [127-129].

4.2 Angiography and Vascular Interventions

In diagnostic and interventional angiography, fluoroscopy guides catheter navigation through vascular systems while administering iodinated contrast to visualize blood flow and detect pathologies such as stenoses, aneurysms, or arteriovenous malformations [130, 131]. Key applications include:

•Coronary angiography: Evaluates atherosclerotic plaques with submillimetre spatial resolution.

•Peripheral angiography: Assesses limb perfusion in critical ischemia.

•Micro angiography: Diagnoses cerebral aneurysms or strokes.

Modern systems employ road-mapping techniques, where a baseline angiogram is superimposed on live fluoroscopy to aid catheter manipulation, reducing procedure time and contrast load.

4.3 Catheter Placement and Guided Procedures

Fluoroscopy is the cornerstone of minimally invasive interventions, including:

•Central venous catheter (CVC) placement: This ensures correct positioning in the superior vena cava.

•Percutaneous nephrostomy: Guides renal access under real-time imaging.

•Electrophysiology studies: Maps cardiac arrhythmias during ablation procedures.

Low-dose protocols and collimation minimize scatter radiation, while last-image-hold (LIH) functions reduce unnecessary exposure.

4.4 Technological Advancements and Safety

The transition from image intensifiers to flat-panel detectors has improved spatial resolution, contrast sensitivity, and dose efficiency. Pulsed fluoroscopy reduces dose by 50–80% compared to continuous modes, and spectral shaping (e.g., copper filtration) optimizes beam quality for specific procedures. Nevertheless, stochastic radiation risks (e.g., cancer) and deterministic effects (e.g., skin injuries in prolonged interventions) necessitate strict adherence to ALARA principles. Emerging innovations like AI-enhanced noise reduction and 3D fluoroscopic navigation (e.g., cone-beam CT fusion) promise to further refine procedural accuracy.

5. Mammography: Advancements in Breast Cancer Screening – Digital Mammography versus 3D Tomosynthesis

Mammography remains the cornerstone of breast cancer screening, demonstrating proven efficacy in early detection and mortality reduction. The transition from screen-film mammography (SFM) to full-field digital mammography (FFDM) and subsequently to digital breast tomosynthesis (DBT, or 3D mammography) represents significant technological evolution, each offering distinct advantages in diagnostic accuracy, workflow efficiency, and radiation dose optimization [132, 133].

5.1 Digital Mammography (FFDM): Technical Basis and Clinical Utility

FFDM utilizes solid-state detectors, typically amorphous selenium or silicon-based, to convert X-rays into electronic signals, which are then reconstructed into high-resolution digital images. Compared to SFM, FFDM provides superior contrast resolution, particularly in dense breast tissue, and enables post-processing enhancements such as window-level adjustments, magnification, and computer-aided detection (CAD) integration. The dose efficiency of FFDM (mean glandular dose ~1.6–2.0 mGy per view) is comparable to or slightly lower than SFM, while eliminating film-processing artifacts. Large-scale trials, including the Digital Mammographic Imaging Screening Trial (DMIST), demonstrated FFDM's improved sensitivity (70–90%) over SFM, particularly in women under 50, premenopausal women, and those with heterogeneously dense or extremely dense breasts (ACR categories C/D) [134-136].

5.2 Digital Breast Tomosynthesis (DBT): Overcoming Structural Overlap

DBT addresses a fundamental limitation of conventional mammography—anatomical noise caused by tissue superposition—by acquiring multiple low-dose projections (typically 9–25) across a limited angular range (15–50°). These projections are reconstructed into 1-mm-thick slices, reducing parenchymal overlap and improving lesion conspicuity [137, 138]. Key advantages include:

•Increased cancer detection rates (CDR): Meta-analyses report a 20–40% increase in invasive cancer detection compared to FFDM alone, particularly for small (<1 cm) and spiculated masses.

•Reduced recall rates: DBT decreases false positives by 15–30%, minimizing unnecessary biopsies and follow-ups.

•Improved assessment of lesion margins and architecture, critical for BI-RADS classification.

However, DBT presents challenges, including longer interpretation times (30–50% increase) and higher radiation doses (combined FFDM+DBT ≈ 2.5–3.5 mGy). Synthetic 2D reconstructions (e.g., C-View™) mitigate dose concerns by eliminating the need for separate FFDM acquisitions.

5.3 Comparative Performance in Screening and Diagnostic Settings

•Screening populations: The TOST and Malmö trials demonstrated DBT's superiority in reducing interval cancers (HR 0.70–0.80), suggesting enhanced early detection.

•Dense breasts: DBT's sensitivity in dense tissue (85–92%) surpasses FFDM (70–80%), though supplemental modalities (e.g., ultrasound, MRI) may still be warranted for high-risk patients.

•Cost-effectiveness: While DBT requires higher initial capital investment, its reduced recall rates may lower long-term healthcare expenditures.

5.4 Emerging Innovations and Future Directions

•AI integration: Deep learning algorithms assist in micro calcification detection and risk stratification (e.g., predicting malignancy likelihood).

•Contrast-enhanced mammography (CEM): Combines iodine-based contrast with FFDM/DBT, offering MRI-like sensitivity in lesion characterization.

•Ultra-low-dose protocols: Photon-counting detectors (PCDs) promise sub-1 mGy exams without compromising image quality.

6.Computed Tomography (CT): Advancements in Cross-Sectional Imaging with Multi-Slice and Contrast-Enhanced Techniques

Computed Tomography (CT) has revolutionized diagnostic imaging by providing high-resolution, cross-sectional anatomical visualization through the integration of X-ray technology and advanced computational reconstruction algorithms. Unlike conventional radiography, which produces superimposed 2D images, CT generates sequential axial slices that can be reformatted into coronal, sagittal, or 3D volumetric images, enabling comprehensive evaluation of complex anatomical structures and pathologies. The evolution from single-slice to multi-slice CT (MSCT) and the development of contrast-enhanced CT (CECT) protocols have significantly expanded clinical applications, improving diagnostic accuracy, temporal resolution, and patient-specific optimization [139-141].

7. Multi-Slice CT (MSCT): Technological Foundations and Clinical Advantages

MSCT, introduced in the late 1990s, employs multiple detector rows (ranging from 4 to 320 slices) to simultaneously capture data during a single gantry rotation [142-144]. This innovation offers several key benefits:

1.Improved Spatial and Temporal Resolution: Modern MSCT systems achieve submillimetre isotropic resolution (0.5–0.625 mm slice thickness), critical for visualizing small structures such as coronary arteries, pulmonary nodules, or subtle fractures. High-speed gantry rotation (<0.3 seconds) reduces motion artifacts, particularly in cardiac or trauma imaging.

2.Extended Anatomical Coverage: MSCT allows rapid acquisition of large volumes (e.g., whole-body trauma scans in <10 seconds), minimizing patient movement and breath-holding requirements.

3.Advanced Post-Processing Capabilities: Multiplanar reconstructions (MPR), maximum intensity projections (MIP), and volume-rendered images enhance diagnostic interpretation in vascular, orthopedic, and oncological imaging.

7.1 Contrast-Enhanced CT (CECT): Mechanisms and Diagnostic Utility

CECT utilizes intravenous (IV) iodinated contrast media to augment tissue contrast, leveraging differences in vascularity and perfusion between normal and pathological tissues [145, 146]. The timing of image acquisition relative to contrast administration is categorized into distinct phases:

•Non-Contrast CT: Baseline assessment of calcifications, hemorrhage, or fat-containing lesions (e.g., adrenal adenomas).

•Arterial Phase (20–30 sec post-injection): Optimal for hyper-vascular lesions (e.g., hepatocellular carcinoma, hyper-enhancing renal masses) and arterial anatomy (e.g., pulmonary embolism, aortic dissection).

•Portal Venous Phase (60–70 sec): Standard for most abdominal evaluations, including liver metastases, pancreatic tumours, and venous thrombosis.

•Delayed Phase (3–5 min): Useful for excretory phase urography or fibrotic tissue characterization.

CECT is indispensable for tumour staging (e.g., RECIST criteria), vascular pathology (e.g., aneurysms, stenoses), and inflammatory conditions (e.g., abscesses, pancreatitis). Dual-energy CT (DECT), an advanced CECT technique, exploits material decomposition algorithms to differentiate iodine, calcium, or uric acid, enabling virtual non-contrast imaging and reducing overall radiation exposure.

8. Clinical Applications and Evidence-Based Outcomes

•Oncology: MSCT with CECT is the backbone of cancer staging (TNM classification), assessing tumour size, lymph node involvement, and distant metastases. Perfusion CT quantifies tumour vascularity, predicting treatment response in glioblastomas or colorectal liver metastases.

•Cardiovascular Imaging: Coronary CT angiography (CCTA) with MSCT detects atherosclerotic plaques with >95% sensitivity, while ECG-gated acquisitions evaluate cardiac function and valve morphology.

•Neuroimaging: Non-contrast CT remains first-line for acute stroke (ASPECTS score), while CECT identifies vascular malformations or tumoral enhancement.

•Trauma: Whole-body MSCT ("pan-scan") is the standard for polytrauma, diagnosing life-threatening injuries (e.g., splenic laceration, pneumothorax) with >90% sensitivity.

8.1 Dose Optimization and Future Directions

Despite its diagnostic power, CT contributes significantly to medical radiation exposure. Strategies to mitigate dose include:

•Iterative reconstruction (IR) and AI-based de-noising algorithms, reducing dose by 30–60% without compromising image quality.

•Protocol personalization based on body habitus and clinical indication (e.g., low-dose lung cancer screening at 1–2 mSv).

•Photon-counting CT (PCCT), an emerging technology offering superior spatial resolution and spectral imaging at reduced doses.

9. Advantages of X-ray Imaging

9.1 Speed and cost-effectiveness

X-ray imaging remains a cornerstone of diagnostic radiology due to its unparalleled speed and cost-effectiveness, making it indispensable in both emergency and routine clinical settings. The acquisition of conventional radiographs typically requires less than 1 second per exposure, enabling rapid assessment of critical conditions such as fractures, pneumothoraces, or bowel obstructions. This efficiency is particularly vital in high-volume environments like emergency departments, where time-sensitive decisions rely on immediate imaging results. Furthermore, modern digital radiography (DR) systems eliminate the need for film processing, reducing examination times to under 5 minutes from image capture to interpretation. Compared to advanced modalities such as MRI or CT, which may require 15–60 minutes per study, X-rays offer a decisive advantage in workflow optimization, particularly for triaging unstable patients [147].

From an economic standpoint, X-ray imaging is a highly resource-efficient diagnostic modality. The initial capital outlay and ongoing operational expenses for radiographic systems are considerably lower than those for cross-sectional modalities such as MRI or CT. For instance, portable X-ray units typically cost between $50,000 and $100,000, which is a fraction of the $1-2 million required for an MRI or CT scanner. This cost-effectiveness, coupled with high diagnostic accuracy for common indications like fracture and pneumonia detection, underscores its significant value. The judicious application of X-rays, guided by evidence-based protocols, ensures optimal resource allocation and strong clinical outcomes, cementing its role as a foundational, cost-effective tool in modern medicine.

9.2 High Spatial Resolution for Bone Structures

X-ray imaging is unparalleled in its ability to provide high spatial resolution for visualizing bone structures, making it the gold standard for diagnosing skeletal pathologies. The modality achieves spatial resolutions of 0.1–0.2 mm, enabling the detection of fine anatomical details such as trabecular patterns, micro fractures, and cortical disruptions that may be imperceptible with other imaging techniques. This precision stems from the differential attenuation of X-rays by calcium-rich bone tissue (effective atomic number, $Z \approx 13.8$), which absorbs photons more efficiently than soft tissues ($Z \approx 7.4$), producing exceptional contrast between osseous and non-osseous structures. As a result, radiographs can delineate subtle fractures, such as hairline fissures in the scaphoid or occult hip fractures, with high diagnostic confidence, guiding timely clinical interventions [51, 147].

The superior resolution of X-rays is particularly evident in extremity and joint imaging, where intricate anatomical relationships must be preserved. For instance, standard hand or wrist radiographs can reveal early erosions in rheumatoid arthritis or subperiosteal resorption in hyperparathyroidism, features critical for disease staging. Similarly, dental radiography leverages this capability to identify periapical abscesses, root fractures, and periodontal bone loss with micron-level precision. Even in comparison to advanced modalities like CT, conventional radiography often provides sharper edge definition for cortical bone evaluation, albeit without cross-sectional capabilities.

Technological advancements, such as digital radiography (DR) with high-frequency generators, have further enhanced spatial resolution while minimizing radiation dose. Post-processing tools, including edge enhancement algorithms and magnification functions, allow radiologists to scrutinize fine bony details without additional exposures. Nevertheless, the modality's limitations in soft-tissue contrast underscore its specialized role in musculoskeletal imaging. When combined with clinical correlation, X-rays' high spatial resolution for bone structures ensures its continued dominance in fracture management, orthopedic planning, and metabolic bone disease assessment.

9.3 Non-invasive (compared to surgery)

X-ray imaging represents a fundamental non-invasive diagnostic modality that provides critical clinical information without the risks associated with surgical exploration. Unlike invasive procedures, which require tissue penetration, anesthesia, and prolonged recovery, radiography enables internal visualization through external energy application (X-ray photons) and detection of transmitted radiation, eliminating the need for incisions or physiological disruption. This non-invasiveness is particularly valuable in acute trauma evaluation, where rapid diagnosis of fractures, dislocations, or pneumothoraces must be achieved without exacerbating patient injury. For example, a simple two-view radiographic series can confirm a femoral neck fracture with >95% sensitivity, obviating the need for diagnostic arthroscopy or exploratory surgery. Similarly, chest X-rays reliably identify pleural effusions or pulmonary consolidations that might otherwise require thoracentesis or biopsy for confirmation.

The non-invasive nature of X-ray imaging also reduces procedure-related complications, including surgical site infections, hemorrhage, or anesthesia-related adverse events. In pediatric populations, where invasive procedures pose heightened risks, radiography serves as a first-line tool for diagnosing congenital hip dysplasia, scoliosis, or non-accidental injuries without subjecting children to unnecessary operative interventions. Furthermore, serial radiographic examinations allow for longitudinal monitoring of conditions such as osteomyelitis or fracture healing, providing repeated assessments without cumulative morbidity.

While advanced modalities like MRI or ultrasound also offer non-invasive alternatives, X-rays maintain distinct advantages in accessibility, speed, and cost-efficiency. Even in cases where soft-tissue evaluation is limited, the combination of radiographic findings with clinical correlation often suffices for definitive diagnosis, avoiding more invasive steps. As low-dose protocols and digital tomosynthesis continue to evolve, the non-invasive benefits of X-ray imaging are further enhanced, reinforcing its role as an indispensable diagnostic tool that balances patient safety with clinical efficacy.

9.4 Widely available in hospitals and clinics

X-ray imaging maintains a dominant position in medical diagnostics due to its near-universal availability across healthcare settings, from tertiary care hospitals to rural clinics. This ubiquity stems from several factors, including relatively low infrastructure requirements, cost-effective implementation, and operational simplicity compared to advanced imaging modalities. Unlike MRI or CT, which demand specialized shielding, cryogenic cooling, or high-power electrical systems, radiographic units can be installed in virtually any clinical space with standard radiation shielding and power supply. Portable X-ray machines further extend accessibility to bedside, emergency, and intraoperative settings, enabling immediate imaging for critically ill or immobile patients.

The widespread adoption of X-ray technology ensures equitable access to diagnostic services, particularly in resource-limited regions where advanced imaging is often unavailable. Serving as a primary tool for critical screenings and trauma evaluations, radiography helps bridge healthcare disparities globally. Even in well-equipped facilities, X-rays remain a vital first-line modality for common conditions, which reduces the burden on costlier and complex services. The technology's simplicity allows a variety of clinicians to perform and interpret basic studies, expediting time-sensitive clinical decisions. The shift to digital radiography (DR) and Picture Archiving and Communication Systems (PACS) has further enhanced this accessibility by enabling rapid image sharing for remote consultations. This, combined with low operational costs and durable hardware, makes X-ray imaging a sustainable and scalable diagnostic solution, solidifying its indispensable role in both routine and emergency care worldwide.

10. Limitations and Risks

10.1 Ionizing radiation exposure (cancer risk, ALARA principle)

Despite its diagnostic utility, X-ray imaging carries inherent risks due to ionizing radiation exposure, which has been linked to stochastic effects (e.g., carcinogenesis) and deterministic effects (e.g., tissue reactions at high doses). The linear no-threshold (LNT) model, widely adopted by regulatory bodies, posits that even low-dose exposure may incrementally increase lifetime cancer risk, particularly for pediatric patients and repeated examinations. Epidemiological studies, such as the BEIR VII report, estimate that 1 mSv of effective dose (equivalent to ~4 chest X-rays) confers a 0.005% increased lifetime risk of fatal cancer, necessitating strict adherence to the ALARA (As Low As Reasonably Achievable) principle [148].

10.2 Radiation risks are tissue- and age-dependent:

•Children exhibit heightened radio sensitivity due to rapidly dividing cells and longer post-exposure lifespans (5–10× greater risk per unit dose than adults).

•Gonadal exposure during pelvic radiography raises concerns about genetic effects, albeit with minimal evidence at diagnostic doses.

•Cumulative exposure in chronic imaging (e.g., serial scoliosis monitoring) may breach 100 mSv, approaching thresholds for measurable cancer risk.

To mitigate these risks, modern protocols emphasize:

•Dose optimization: Use of low kVp/high mAs for high-contrast exams (e.g., bone imaging) and high kVp for chest studies to reduce skin dose.

•Collimation and shielding: Thyroid shields (for dental X-rays) and lead aprons for radiosensitive tissues.

•Alternative modalities: Ultrasound or MRI for pediatric and obstetric imaging when feasible.

While the absolute risk remains small compared to clinical benefits, ongoing advancements in digital detectors, iterative reconstruction, and AI-driven dose reduction continue to refine X-ray safety.

10.3 Poor soft-tissue contrast (compared to MRI/ultrasound)

One of the most significant limitations of X-ray imaging is its poor soft-tissue contrast resolution, particularly when compared to advanced modalities such as magnetic resonance imaging (MRI) and ultrasound. This constraint arises from the fundamental physics of X-ray interactions with biological tissues, where attenuation differences between soft-tissue structures (e.g., muscles, tendons, and organs) are often minimal, resulting in low-contrast differentiation. Unlike MRI, which exploits variations in proton relaxation times to generate high soft-tissue contrast, or ultrasound, which uses acoustic impedance differences, X-ray imaging relies primarily on density and atomic number disparities, which are less pronounced in non-calcified tissues. Consequently, pathologies such as ligamentous injuries, brain parenchyma abnormalities, or early-stage tumors may remain undetectable on conventional radiographs.

The clinical implications of these limitations are significant. In neurological imaging, for instance, X-rays are unable to visualize intracranial structures, rendering them ineffective for diagnosing conditions such as strokes, gliomas, or demyelinating diseases, all of which require advanced modalities like MRI or CT for accurate assessment. Similarly, in musculoskeletal imaging, while X-rays are highly effective for detecting fractures, their poor sensitivity for non-osseous pathologies like ligament tears, meniscal injuries, or early-stage stress fractures necessitates the use of more advanced cross-sectional techniques. This limitation also extends to oncology, where X-rays are restricted to identifying advanced bony metastases and cannot characterize soft-tissue tumours, a task for which modalities like CT, MRI, or PET-CT are essential. Ultimately, despite its utility as a first-line tool, the limited soft-tissue contrast of X-ray imaging requires the use of other advanced techniques for the definitive diagnosis of many conditions. They often fail to reveal meniscal tears, rotator cuff injuries, or bone marrow edema, necessitating supplementary MRI examinations. In abdominal imaging, radiographs provide limited information about solid organ pathology (e.g., liver lesions or pancreatic masses), where ultrasound or contrast-enhanced CT is preferred.

Technological advancements like digital tomosynthesis and dual-energy subtraction have partially improved tissue differentiation in X-ray imaging, though they do not achieve the soft-tissue resolution of MRI. Efforts to enhance contrast through increased radiation dose are also constrained by the ALARA (As Low As Reasonably Achievable) principle, as higher exposure does not yield a proportional improvement in soft-tissue resolution. Consequently, while X-rays are indispensable for bone and pulmonary imaging and acute trauma, their diagnostic utility for soft-tissue applications remains limited, reinforcing the necessity of a multimodal approach for comprehensive patient care.[149].

10.4 Limited 3D visualization (unless using CT)

A fundamental constraint of conventional X-ray imaging lies in its inherent two-dimensional projection geometry, which results in limited three-dimensional visualization of anatomical structures. This limitation stems from the physical principle of superimposition, where all tissues along the X-ray beam path are compressed into a single planar image. Consequently, critical spatial relationships between structures may be obscured, potentially compromising diagnostic accuracy. The superposition effect is particularly problematic in complex anatomical regions such as the chest (where ribs may obscure pulmonary nodules), the spine (where vertebral elements overlap), and the skull (where multiple bony structures intersect). This 2D limitation contrasts sharply with computed tomography (CT), which provides true cross-sectional imaging through volumetric acquisition and reconstruction algorithms.

The clinical implications of this dimensional constraint are significant. In fracture assessment, for instance, non-displaced fractures may be missed in up to 15-20% of cases when relying solely on conventional radiography, particularly in anatomically complex areas like the scaphoid or femoral neck. Similarly, in pulmonary imaging, the sensitivity for detecting small (<1 cm) lung nodules decreases substantially compared to CT, with studies demonstrating up to 25% of potentially malignant nodules being overlooked on chest radiographs. The superimposition problem also complicates the evaluation of organ size and precise lesion localization, often necessitating additional views or follow-up imaging. While specialized techniques such as stereoscopic radiography or digital tomosynthesis attempt to address this limitation by providing pseudo-3D information, they cannot match the spatial resolution and true volumetric data acquisition of CT. The development of dual-energy subtraction radiography has provided some improvement in tissue differentiation, but fundamental 3D relationships remain challenging to ascertain. This dimensional limitation becomes particularly consequential in surgical planning, radiation therapy targeting, and complex fracture management, where precise spatial understanding is paramount. Modern solutions to this challenge include the integration of artificial intelligence (AI) algorithms to reconstruct three-dimensional information from two-dimensional projections, as well as the increased use of cone-beam computed tomography (CT) in specialized fields like dentistry and orthopedics. However, these approaches still face obstacles in widespread clinical adoption, primarily due to concerns regarding cost-effectiveness and radiation dose. Therefore, while conventional radiography remains a vital tool for initial screening, its inherent dimensional constraints often require supplemental advanced imaging for a comprehensive evaluation, especially in complex clinical cases.10.5 Challenges in obese patients or overlapping structures.

10.5 Challenges in obese patients or overlapping structures

X-ray imaging faces significant diagnostic limitations when evaluating obese patients or anatomically complex regions where structures overlap. In obese individuals, increased adipose tissue thickness results in greater X-ray attenuation and scatter radiation, which degrades image quality by reducing contrast resolution and increasing noise. The higher photon absorption in larger body habitus often necessitates increased technical parameters (e.g., higher kVp and mAs), leading to elevated radiation doses while still producing suboptimal images. Additionally, physical constraints, such as table weight limits and detector size, may prevent proper positioning, further compromising diagnostic accuracy. Studies indicate that radiographic sensitivity for detecting pulmonary nodules, fractures, or abdominal pathologies decreases by 15–30% in obese patients compared to those with normal body mass indices (BMIs), often necessitating alternative imaging modalities like CT or ultrasound [150-152].

Overlapping anatomical structures present another major challenge, particularly in chest, abdominal, and skeletal imaging. In standard two-dimensional radiography, superimposition of bones, organs, or foreign objects can obscure critical findings. For example, ribs overlapping lung lesions may mask early-stage tumours, while intestinal gas patterns in abdominal X-rays can mimic or conceal bowel obstructions. Similarly, in spinal imaging, the complex 3D arrangement of vertebrae makes it difficult to assess alignment, fractures, or degenerative changes without additional oblique or lateral views. While specialized projections (e.g., lordotic views for lung apices) or digital tomosynthesis can mitigate some of these limitations, they do not fully replicate the diagnostic precision of cross-sectional imaging [153, 154].

To address these challenges, modern advancements such as dual-energy subtraction, AI-assisted image enhancement, and weight-adaptive exposure algorithms are being implemented. However, fundamental physical constraints persist, reinforcing the need for judicious modality selection—particularly in obese populations or when evaluating anatomically crowded regions—to ensure diagnostic efficacy while minimizing unnecessary radiation exposure.

11. Recent Technological Advances

11.1 Digital radiography (DR) vs. traditional film.

The transition from traditional film-based radiography to digital radiography (DR) represents a significant technological evolution in medical imaging, offering substantial improvements in image quality, workflow efficiency, and dose optimization. Traditional screen-film radiography (SFR) relied on photochemical processes, where X-ray photons exposed silver halide crystals in film emulsion, requiring chemical development to produce a visible image. While SFR provided high spatial resolution (~10 lp/mm), its limitations included a narrow dynamic range, irreversible image acquisition, and inconsistent optical density due to processing variability. In contrast, DR systems utilize solid-state detectors—either indirect conversion (scintillator + photodiode arrays) or direct conversion (amorphous selenium) to transform X-ray energy directly into digital signals. This shift enables wider dynamic range, post-processing enhancement, and immediate image availability, significantly improving diagnostic versatility

DR offers several key advantages over traditional film. First, its dose efficiency reduces patient exposure by 30–50% while maintaining diagnostic quality, as digital detectors exhibit superior quantum detection efficiency (DQE) compared to film-screen combinations [155-157]. Second, advanced post-processing tools such as window-level adjustment, edge enhancement, and noise reduction allow radiologists to optimize images retrospectively without repeat exposures, a critical benefit in pediatric and trauma imaging. Third, DR eliminates film storage and chemical processing, integrating seamlessly with Picture Archiving and Communication Systems (PACS) for streamlined workflow and telemedicine applications.

However, DR is not without challenges. The initial capital cost of DR systems remains higher than film-based setups, and spatial resolution, while sufficient for most clinical applications, is theoretically lower (~3–5 lp/mm) than high-detail film. Nevertheless, the diagnostic superiority of DR in low-contrast scenarios (e.g., chest or abdominal imaging) and its integration with AI-based analytics for automated abnormality detection have cemented its dominance in modern radiology. As DR technology continues to advance, with developments like portable wireless detectors and dual-energy subtraction, it further displaces traditional film, reinforcing its role as the standard for contemporary radiographic practice [158].

11.2 AI-assisted image analysis (automated fracture detection, pneumonia screening)

The integration of artificial intelligence (AI) into radiographic image analysis represents a transformative advancement in medical imaging, particularly in automated fracture detection and pneumonia screening. AI algorithms, primarily based on deep learning convolutional neural networks (CNNs), have demonstrated remarkable accuracy in interpreting complex imaging data, augmenting diagnostic precision and workflow efficiency. In fracture detection, AI systems trained on large datasets of annotated radiographs can identify subtle cortical disruptions, trabecular fractures, and misalignments with sensitivity exceeding 90% in some studies, approaching the performance of experienced radiologists. These tools are particularly valuable in high-volume emergency departments, where they serve as "second readers" to reduce oversight of occult fractures in anatomically complex regions like the wrist, hip, or spine. Similarly, for pneumonia screening, AI models analyse chest X-rays to detect consolidations, interstitial opacities, and pleural effusions, with some algorithms achieving area-under-the-curve (AUC) values >0.95 in distinguishing bacterial from viral pneumonias—a critical distinction for guiding antibiotic therapy [159, 160].

The implementation of AI-assisted diagnostics follows two paradigms: computer-aided detection (CADe), which flags potential abnormalities for radiologist review, and computer-aided diagnosis (CADx), which provides probabilistic assessments of pathology. Both approaches leverage transfer learning from pre-trained models (e.g., ResNet, DenseNet) adapted to medical imaging. However, challenges persist, including dataset bias (underrepresentation of rare fractures or atypical pneumonias), "black box" interpretability (limited insight into AI decision pathways), and integration barriers with existing PACS workflows. Regulatory frameworks, such as the FDA's 510(k) clearance for AI radiology devices, are evolving to address these concerns while ensuring clinical safety.

Future directions include multimodal AI combining radiographs with electronic health records for context-aware analysis and edge computing for real-time processing in resource-limited settings. As these technologies mature, AI-assisted image analysis is poised to become a standard adjunct in radiology, enhancing diagnostic accuracy while mitigating interpreter fatigue and variability.

11.3 Low-dose X-ray techniques (pediatric imaging)

The development of low-dose X-ray techniques represents a critical advancement in pediatric radiology, addressing the heightened radio sensitivity of children while maintaining diagnostic efficacy. Children possess rapidly dividing cells and longer post-exposure lifespans, making them 5–10 times more vulnerable to radiation-induced stochastic effects than adults. Traditional pediatric protocols already employ weight- and age-adjusted exposure parameters, but recent innovations have further reduced doses without compromising image quality. Advanced iterative reconstruction algorithms, such as model-based iterative reconstruction (MBIR), enable 30–70% dose reduction compared to conventional filtered back projection by suppressing noise while preserving anatomical detail. Similarly, photon-counting detectors (PCDs), an emerging technology, improve dose efficiency through energy-selective imaging, eliminating electronic noise and enhancing contrast-to-noise ratios at ultra-low doses (e.g., <0.1 mSv for chest radiographs) [161, 162].

Clinical implementations include spectral shaping with copper or silver filters to remove low-energy photons that contribute to skin dose but not image formation, and adaptive collimation to minimize scattered radiation. In digital radiography (DR), artificial intelligence (AI)-based de-noising tools trained on pediatric datasets recover diagnostic information from low-exposure images, with studies demonstrating equivalent accuracy at 50% lower doses. For fluoroscopic procedures (e.g., voiding cystourethrograms), pulse-rate reduction (to 4–7.5 fps) coupled with last-image-hold functionality cuts doses by 60–80% [163, 164].

These advances align with the Image Gently® campaign guidelines, which advocate for ALARA (As Low As Reasonably Achievable) compliance in pediatric imaging. However, challenges persist in standardizing protocols across institutions and ensuring diagnostic confidence at ultra-low doses for subtle pathologies (e.g., non-displaced fractures or early pneumonia). Future directions include deep learning-based dose prediction systems that customize exposures based on individual patient anatomy and clinical indication, potentially achieving sub-micro Sievert examinations for routine screenings.

11.4 Portable and point-of-care X-ray devices (e.g., in ICUs)

The emergence of portable and point-of-care X-ray devices has revolutionized diagnostic imaging in intensive care units (ICUs), enabling bedside radiographic evaluation of critically ill patients who cannot be safely transported to fixed imaging suites. Modern portable systems incorporate lightweight, wireless flat-panel detectors and battery-powered X-ray tubes, achieving diagnostic quality comparable to stationary units while operating at lower radiation doses (typically 2–3 mGy per chest examination). These devices are particularly vital for monitoring ventilator-associated pneumonia (VAP), pneumothorax, endotracheal tube positioning, and line placements, with studies demonstrating >95% concordance between portable and fixed-unit radiographs for critical findings [165, 166].

Technological refinements have enhanced the utility of point-of-care radiography in ICUs. Motorized collimation and automatic exposure control (AEC) [167] optimize image quality while minimizing scatter radiation in crowded clinical environments. AI-powered image enhancement algorithms compensate for suboptimal positioning (common in immobile patients) by correcting rotation and magnification artifacts in real time. Some advanced portable systems now integrate dual-energy imaging, allowing bedside tissue decomposition (e.g., lung vs. bone visualization) without patient repositioning—a capability previously limited to fixed DR systems.

Infection control has driven innovation in disposable detector covers and UV-C decontamination cycles, reducing nosocomial transmission risks in immunocompromised populations. Wireless DICOM transmission via hospital networks enables immediate interpretation by off-site radiologists, expediting time-sensitive decisions. However, challenges remain in standardizing exposure protocols across diverse patient sizes and ICU settings, and in minimizing occupational exposure to staff during frequent bedside imaging. Future developments include robotic portable systems for autonomous positioning and ultra-low-field portable CT hybrids to bridge the gap between radiography and cross-sectional imaging at the point of care.

12. Future Perspectives

12.1 Integration with AI for faster, more accurate diagnoses.

The integration of artificial intelligence (AI) into radiographic imaging is poised to revolutionize diagnostic workflows by enabling faster, more accurate, and standardized interpretations. AI algorithms, particularly deep learning convolutional neural networks (CNNs), have demonstrated remarkable potential in automating image analysis, reducing interpretation times, and detecting subtle pathologies that may elude human observers. In fracture detection, for instance, AI-assisted systems have achieved sensitivity rates exceeding 95% for identifying subtle cortical disruptions and occult fractures, significantly reducing missed diagnoses in high-volume emergency settings. Similarly, in chest radiography, AI models trained on vast datasets can flag pulmonary nodules, consolidations, and pneumothoraces with accuracy comparable to experienced radiologists, while simultaneously prioritizing urgent cases for expedited review [168].

Beyond detection, AI facilitates quantitative analysis—measuring tumour growth, tracking fracture healing, or calculating cardiothoracic ratios—with precision unattainable through manual methods. Natural language processing (NLP) further enhances efficiency by automatically generating structured reports from radiologist dictations, minimizing administrative burdens. However, challenges such as algorithmic bias (due to the underrepresentation of rare conditions in training data), regulatory hurdles, and the need for human oversight persist. Future advancements will likely focus on explainable AI (XAI), which provides transparent decision-making pathways to build clinician trust, and federated learning, enabling collaborative model training across institutions without compromising patient privacy.

As AI becomes seamlessly embedded in picture archiving and communication systems (PACS), its role will expand from assistive tools to proactive diagnostic partners, offering real-time decision support and predictive analytics. Ultimately, AI integration promises to enhance diagnostic consistency, reduce radiologist burnout, and improve patient outcomes through earlier and more accurate detection of critical conditions.

12.2 Advances in photon-counting CT

Photon-counting computed tomography (PCCT) represents a transformative advancement in medical imaging, offering superior spatial and contrast resolution while simultaneously reducing radiation exposure compared to conventional energy-integrating detector (EID) CT systems. By directly converting X-ray photons into electrical signals and categorizing them by energy levels, PCCT eliminates electronic noise and enables multi-energy spectral imaging without the need for dual-source configurations. This technology achieves spatial resolutions up to 150–200 μm, allowing visualization of previously imperceptible microstructural details in coronary plaques, pulmonary nodules, and trabecular bone. Clinical studies demonstrate PCCT's ability to differentiate calcium, iodine, and uric acid with high specificity, facilitating precise tissue characterization in oncologic, vascular, and musculoskeletal applications [169].

Key innovations in PCCT include virtual non-contrast imaging, which reduces patient dose by obviating separate pre-contrast scans, and K-edge imaging, which enhances material separation for novel contrast agents. Early trials in coronary artery imaging show PCCT's potential to identify vulnerable plaques through lipid-core detection, while ultra-high-resolution lung scans improve early-stage lung cancer diagnosis. Additionally, PCCT's inherent spectral capabilities enable quantitative biomarkers for tissue perfusion and fibrosis, advancing precision medicine [170, 171].

Despite these advantages, challenges remain in scalability, cost, and workflow integration, particularly in adapting reconstruction algorithms for spectral data. Future developments aim to miniaturize detector technology for broader clinical adoption and leverage artificial intelligence for optimized image reconstruction and dose management. As PCCT evolves, it is poised to redefine diagnostic paradigms, offering unparalleled detail at lower doses, ultimately improving patient outcomes across multiple specialties.

12.3 Potential of phase-contrast and dark-field X-ray imaging

Emerging X-ray imaging techniques, particularly phase-contrast imaging (PCI) and dark-field imaging (DFI), represent a paradigm shift in medical diagnostics by exploiting previously untapped physical properties of X-ray interactions with biological tissues. Unlike conventional absorption-based radiography, which relies on differential X-ray attenuation, PCI detects phase shifts in X-ray waves as they pass through tissues, rendering visible subtle density variations in soft tissues that exhibit minimal absorption contrast. This technique enhances visualization of low-contrast structures such as tendons, ligaments, and early-stage tumours, with preclinical studies demonstrating up to 1000-fold improvement in soft-tissue contrast compared to traditional radiography. Meanwhile, DFI measures small-angle scattering from sub-pixel microstructures, providing complementary information about tissue composition at the cellular or fibrillary level—particularly valuable for assessing pulmonary microstructure, cartilage degeneration, and breast calcifications [172-174].

Current research highlights PCI's potential in neurological imaging, where it can differentiate white and gray matter without contrast agents, and in breast cancer screening, where it improves the detection of micro-calcifications and ductal abnormalities [175]. DFI, on the other hand, has shown promise in chronic lung disease diagnostics, identifying emphysema and fibrosis through characteristic scattering patterns invisible to conventional CT. Synchrotron-based studies have achieved sub-micron spatial resolution, though translation to clinical settings requires overcoming challenges in source compactness and acquisition speed.

The integration of grating-based interferometry now enables PCI and DFI with conventional X-ray tubes, paving the way for clinical adoption. Future advancements aim to combine these modalities with photon-counting detectors and AI-based reconstruction, potentially enabling multi-contrast imaging in a single scan. While technical hurdles remain in dose optimization and system portability, phase-contrast and dark-field X-ray imaging hold transformative potential for early disease detection and personalized medicine, bridging the resolution and contrast gaps between radiography and histopathology [176, 177].

12.4 Reducing radiation dose while improving image quality.

Driven by the paramount objective of reducing radiation exposure while enhancing image quality, modern radiography has leveraged technological innovations and protocol optimization. Photon-counting detectors (PCDs), for instance, significantly improve dose efficiency and enable multi-energy imaging for superior tissue differentiation. Similarly, iterative reconstruction algorithms, including those based on deep learning, preserve diagnostic fidelity at doses 50-70% lower than traditional methods. Furthermore, AI-driven exposure control systems and ultra-low-dose protocols, supported by neural network de-noising, now dynamically tailor doses to specific patient anatomy, pushing the boundaries of safe imaging. Emerging techniques like phase-contrast and dark-field imaging also offer the potential for dose-neutral soft-tissue visualization. While challenges remain in standardizing these innovations and ensuring regulatory compliance, ongoing research aims to diminish the trade-off between dose and image quality, enabling safer and more precise radiography across all patient populations [178, 179].

13. Conclusion

X-ray imaging remains a cornerstone of modern medicine due to its unique combination of speed, cost-effectiveness, and high spatial resolution for bone structures. This makes it an indispensable tool for rapid trauma assessment, fracture detection, and pulmonary screening, particularly in emergency and critical care settings. Its widespread availability and affordability also ensure equitable diagnostic access, from urban hospitals to rural clinics, securing its vital role in global health. Despite inherent limitations like ionizing radiation exposure, poor soft-tissue contrast, and 2D anatomical superimposition, significant advancements have fortified the modality. Digital radiography (DR) and sophisticated low-dose protocols have enhanced image quality and patient safety, while AI-assisted image analysis has improved diagnostic accuracy and streamlined workflows. Innovations such as portable and point-of-care X-ray systems have extended its utility to intensive care and remote environments. Future developments promise to further overcome these challenges. Technologies like photon-counting detectors and phase-contrast imaging are expected to provide superior tissue characterization and mitigate traditional soft-tissue limitations. The growing integration of artificial intelligence will enable more automated diagnostics and personalized dose optimization. As research continues to refine these techniques and address persistent issues like dose management and 3D visualization constraints, X-ray imaging will further solidify its role as a foundational tool, bridging its historical reliability with cutting-edge innovation to support precision diagnostics and personalized healthcare.

14. References

[1] S. Arati, Panchbhai "Wilhelm Conrad Röntgen and the discovery of X-rays: Revisited after centennial," vol. 27,1, pp. 90-95, 2015.

[2] R. R. Babic, G. S. Babic, S. R. Babic., "120 Years Since the discovery of X-Rays/120. Godina od otkrica X-Zraka," vol. 69,9-10, pp. 323-331, 2016.

[3] PM Dunn, and n. edition, "Wilhelm Conrad Röentgen (1845–1923), the discovery ofx rays and perinatal diagnosis," vol. 84,2, pp. F138-F139, 2001.

[4] F. J. P. M. Nüsslin, "Wilhelm Conrad Röntgen: The scientist and his discovery," vol. 79, pp. 65-68, 2020.

[5] RF Mould, and Biology, "The early history of x-ray diagnosis with emphasis on the contributions of physics 1895-1915," Phys Med Biol vol. 40,11, pp. 1741, 1995.

[6] UF Rosenow, "Notes on the legacy of the Röntgen rays," vol. 22,11, pp. 1855-1867, 1995.

[7] A. Stewart, W. Pennybacker, and R. J. B. M. J. Barber, "Adult leukaemias and diagnostic x rays," Br Med J vol. 2,5309, pp. 882, 1962.

[8] M. Godfrey Hochbaum, "Why people seek diagnostic x-rays," Public Health Rep (1896) vol. 71,4, pp. 377, 1956.

[9]G.M Ardran, Mathematical, and P. Sciences, "The application and limitation of the use of X-rays in medical diagnosis," Philos Trans R Soc, vol. 292,1390, pp. 147-156, 1979.

[10] E. T. Parks, and G. F. J. J. C. D. P. Williamson, “Digital radiography: an overview,” J Contemp Dent Pract vol. 3,4, pp. 23-39, 2002.

[11] J. J. V. Mattoon, C. Orthopaedics, and Traumatology, “Digital radiography,” Vet Comp Orthop Traumatol vol. 19,03, pp. 123-132, 2006.

[12] M. Korner, C. H. Weber, S. Wirth et al., “Advances in digital radiography: physical principles and system overview,” Radiographics vol. 27,3, pp. 675-686, 2007.

[13] F. Paul, van der Stelt, “Better imaging: the advantages of digital radiography,” J Am Dent Assoc vol. 139, pp. S7-S13, 2008.

[14] T. M. Buzug, "Computed tomography," Springer handbook of medical technology, pp. 311-342: Springer, 2011.

[15] M. Mazonakis, and J. J. E. j. o. r. Damilakis, “Computed tomography: What and how does it measure?” vol. 85,8, pp. 1499-1504, 2016.

[16] Sharon L. Brooks, “Computed tomography,” Dent Clin North Am vol. 37,4, pp. 575-590, 1993.

[17] P. Shrimpton, M. Hillier, M. Lewis et al., Doses from computed tomography (CT) examinations in the UK-2003 review: NRPB Chilton, 2005.

[18] M. J. R. Mahesh, “Fluoroscopy: patient radiation exposure issues,” Radiographics vol. 21,4, pp. 1033-1045, 2001.

[19] D. Miller, “Overview of contemporary interventional fluoroscopy procedures,” Health Phys vol. 95,5, pp. 638-644, 2008.

[20] B. Daly, and P. A. J. R. Templeton, “Real-time CT fluoroscopy: evolution of an interventional tool,” Radiology vol. 211,2, pp. 309-315, 1999.

[21] E. Ron, “Cancer risks from medical radiation,” Health Phys vol. 85,1, pp. 47-59, 2003.

[22] M. S. Linet, T. L. Slovis, D. L. Miller et al., “Cancer risks associated with external radiation from diagnostic imaging procedures,” CA Cancer J Clin vol. 62,2, pp. 75-100, 2012.

[23] D. J. Brenner, and E. J. J. T. l. Hall, “Risk of cancer from diagnostic X-rays,” Lancet vol. 363,9427, pp. 2192, 2004.

[24] E. Karavas, B. Ece, S. Aydın et al., “Are we aware of radiation: A study about necessity of diagnostic X-ray exposure,” vol. 12,4, pp. 264, 2022.

[25] S. O. Hansson, “Improvement principles,” J Safety Res vol. 69, pp. 33-41, 2019.

[26] S. O. Hansson, "Zero visions and other safety principles," The Vision Zero Handbook: Theory, Technology and Management for a Zero Casualty Policy, pp. 1-75: Springer, 2022.

[27] P. A. Bryant, “Radiation Protection Optimisation in New Nuclear Build: Challenges in the application of the As Low As Reasonably Achievable (ALARA) Principle,” University of Surrey, 2021.

[28] N. F. A. Nor Azman, S. A. Othman, N. F. Abu Bakar et al., “Safety culture in handling radioactive materials: a review,” 2018.

[29] A. Clement David-Olawade, D. B. Olawade, L. Vanderbloemen et al., “AI-Driven Advances in Low-Dose Imaging and Enhancement—A Review,” vol. 15,6, pp. 689, 2025.

[30] I.-S. Tzeng, P.-C. Hsieh, W.-L. Su et al., “Artificial Intelligence-assisted chest X-ray for the diagnosis of COVID-19: A systematic review and meta-analysis,” Diagnostics (Basel), vol. 13,4, pp. 584, 2023.

[31] R. V. Gupta, M. K. Kalra, S. Ebrahimian et al., “Complex relationship between artificial intelligence and CT radiation dose,” Academic Radiology vol. 29,11, pp. 1709-1719, 2022.

[32] S. Schumann, B. Thelen, S. Ballestra et al., “X-ray image calibration and its application to clinical orthopedics,” Med Eng Phys vol. 36,7, pp. 968-974, 2014.

[33] K. Mori, N. Sekine, H. Sato et al., “Application of synchrotron X-ray imaging to phase objects in orthopedics,” J Synchrotron Radiat vol. 9,3, pp. 143-147, 2002.

[34] A. M. Davies, and H. Pettersson, Orthopedic imaging: techniques and applications: Springer Science & Business Media, 2012.

[35] M. K. Santos, J. Elias Júnior, F. M. Mauad et al., “Magnetic resonance imaging of the chest: current and new applications, with an emphasis on pulmonology,” J Bras Pneumol vol. 37,2, pp. 242-258, 2011.

[36] I. N. Wijma, R. F. Casal, G. Z. Cheng et al., “Radiation Principles, Protection, and Reporting for Interventional Pulmonology: A World Association of Bronchology and Interventional Pulmonology White Paper,” Respiration vol. 103,11, pp. 707-721, 2024.

[37] R. Vliegenthart, A. Fouras, C. Jacobs et al., “Innovations in thoracic imaging: CT, radiomics, AI and x-ray velocimetry,” Respirology vol. 27,10, pp. 818-833, 2022.

[38] S. Oprea, C. Marinescu, I. Lita et al., "Image processing techniques used for dental x-ray image analysis." pp. 125-129.

[39] A. Kumar, H. S. Bhadauria, and A. J. P. C. S. Singh, "Descriptive analysis of dental X-ray images using various practical methods: A review," Peerj Computer Science vol. 7, pp. e620, 2021.

[40] M. Uo, T. Wada, and T. J. J. D. S. R. Sugiyama, "Applications of X-ray fluorescence analysis (XRF) to dental and medical specimens," Japanese Dental Science Review vol. 51,1, pp. 2-9, 2015.

[41] L. Yang, L.-g. Ye, J.-b. Ding et al., "Use of a full-body digital X-ray imaging system in acute medical emergencies: a systematic review," Emerg Med J vol. 33,2, pp. 144-151, 2016.

[42] E. Fatihoglu, S. Aydin, F. D. Gokharman et al., "X-ray use in chest imaging in emergency department on the basis of cost and effectiveness," Acad Radiol vol. 23,10, pp. 1239-1245, 2016.

[43] R. Khan, S. Siddique, F. Jabeen et al., "Role of chest X-ray and Lung Ultrasound in diagnosis and treatment of Children and Infants with Pneumonia," vol. 27,4, pp. 352-363, 2021.

[44] M. Elsharkawy, A. Sharafeldeen, F. Taher et al., "Early assessment of lung function in coronavirus patients using invariant markers from chest X-rays images," Sci Rep vol. 11,1, pp. 12095, 2021.

[45] W. Y. N. Naing, Z. Z. J. S. Htike, and I. Processing, "Advances in automatic tuberculosis detection in chest x-ray images," vol. 5,6, pp. 41, 2014.

[46] S. A Patil, and Citeseer "Texture analysis of TB X-ray images using image processing techniques," vol. 3,1, pp. 53-56, 2012.

[47] E. L. Irede, O. R. Aworinde, O. K. Lekan et al., "Medical imaging: a critical review on X-ray imaging for the detection of infection," pp. 1-45, 2024.

[48] B. Jany, and T. Welte, "Pleural effusion in adults—etiology, diagnosis, and treatment," vol. 116,21, pp. 377, 2019.

[49] J. E. Heffner, J. S. Klein, and C. J. C. Hampson, "Diagnostic utility and clinical application of imaging for pleural space infections," Chest vol. 137,2, pp. 467-479, 2010.

[50] J. M. Porcel, M. Azzopardi, C. Koegelenberg et al., "The diagnosis of pleural effusions," Expert Rev Respir Med vol. 9,6, pp. 801-815, 2015.

[51] D. Pfeiffer, F. Pfeiffer, and E. J. M. I. i. O. Rummeny, "Advanced X-ray imaging technology," Recent Results Cancer Res vol. 216, pp. 3-30, 2020.

[52] J. A. Seibert, "Projection x-ray imaging: Radiography, mammography, fluoroscopy," Health Phys vol. 116,2, pp. 148-156, 2019.

[53] P. C. Johns, and M. J. J. M. p. Yaffe, "Theoretical optimization of dual-energy x-ray imaging with application to mammography," Med Phys vol. 12,3, pp. 289-296, 1985.

[54] A. Karellas, and S. J. M. p. Vedantham, "Breast cancer imaging: a perspective for the next decade," Med Phys vol. 35,11, pp. 4878-4897, 2008.

[55] Z. S. Lima, M. R. Ebadi, G. Amjad et al., "Application of imaging technologies in breast cancer detection: a review article," Open Access Maced J Med Sci vol. 7,5, pp. 838, 2019.

[56] S. Di Maria, S. Vedantham, and P. J. E. J. o. R. Vaz, "X-ray dosimetry in breast cancer screening: 2D and 3D mammography," Eur J Radiol vol. 151, pp. 110278, 2022.

[57] A. C. Lardo, "Real-time magnetic resonance imaging: diagnostic and interventional applications," Pediatr Cardiol vol. 21,1, pp. 80-98, 2000.

[58] M. Diana, P. Halvax, B. Dallemagne et al., "Real-time navigation by fluorescence-based enhanced reality for precise estimation of future anastomotic site in digestive surgery," Surg Endosc vol. 28,11, pp. 3108-3118, 2014.

[59] G. Katti, S. A. Ara, and A. J. I. j. o. d. c. Shireen, "Magnetic resonance imaging (MRI)–A review," vol. 3,1, pp. 65-70, 2011.

[60] T. Dill, "Contraindications to magnetic resonance imaging," Heart vol. 94,7, pp. 943-948, 2008.

[61] P. N. T. Wells, and biology, "Ultrasound imaging," Phys Med Biol vol. 51,13, pp. R83, 2006.

[62] M. A. Schellpfeffer, "Ultrasound imaging in research and clinical medicine," Birth Defects Res C Embryo Today vol. 99,2, pp. 83-92, 2013.

[63] N. Pace, L. Ricci, and S. J. S. Negrini, "A comparison approach to explain risks related to X-ray imaging for scoliosis, 2012 SOSORT award winner," Scoliosis vol. 8,1, pp. 1-7, 2013.

[64] D. F. Regulla, and H. J. R. p. d. Eder, "Patient exposure in medical X-ray imaging in Europe," Radiat Prot Dosimetry vol. 114,1-3, pp. 11-25, 2005.

[65] U. Arndt, "Generation of X-rays," 2006.

[66] H. Hayashi, N. Kimoto, T. Asahara et al., "Photon counting detectors for x-ray imaging," vol. 10, pp. 978-973, 2021.

[67] H. A. Kramers, Edinburgh, D. P. Magazine, and J. o. Science, "XCIII. On the theory of X-ray absorption and of the continuous X-ray spectrum," vol. 46,275, pp. 836-871, 1923.

[68] P. Gorenstein, H. Gursky, and G. J. A. J. Garmire, vol. 153, p. 885, “The analysis of X-ray spectra,” vol. 153, pp. 885, 1968.

[69] J. A. Seibert, “X-ray imaging physics for nuclear medicine technologists. Part 1: Basic principles of x-ray production,” J Nucl Med Technol vol. 32,3, pp. 139-147, 2004.

[70] P. Russo, “2.01 Physical basis of X-ray imaging,” pp. 1-48, 2014.

[71] S. Kulpe, M. Dierolf, B. Günther et al., “Spectroscopic imaging at compact inverse Compton X-ray sources,” Physica Medica-European Journal of Medical Physics vol. 79, pp. 137-144, 2020.

[72] G. Harding, B. J. R. p. Schreiber, and chemistry, “Coherent X-ray scatter imaging and its applications in biomedical science and industry,” Radiation Physics and Chemistry vol. 56,1-2, pp. 229-245, 1999.

[73] T. J. Petrone, Energy optimization and scatter in chest radiography: Rutgers The State University of New Jersey, School of Graduate Studies, 1995.

[74] P. E. Kinahan, B. H. Hasegawa, and T. Beyer, "X-ray-based attenuation correction for positron emission tomography/computed tomography scanners." pp. 166-179.

[75] K. LaCroix, B. Tsui, B. Hasegawa et al., “Investigation of the use of X-ray CT images for attenuation compensation in SPECT,” Ieee Transactions on Nuclear Science vol. 41,6, pp. 2793-2799, 1994.

[76] N. Kotwaliwale, P. R. Weckler, and G. H. J. B. e. Brusewitz, “X-ray attenuation coefficients using polychromatic X-ray imaging of pecan components,” Biosystems Engineering vol. 94,2, pp. 199-206, 2006.

[77] G. L. Locher, “The compound photoelectric effect of X-rays in light elements,” Physical Review vol. 40,4, pp. 484, 1932.

[78] H. Hall, “The theory of photoelectric absorption for x-rays and γ-rays,” vol. 8,4, pp. 358, 1936.

[79] C.-K. Qiao, J.-W. Wei, and L. J. C. Chen, “An overview of the compton scattering calculation,” Crystals vol. 11,5, pp. 525, 2021.

[80] R. Pratt, L. LaJohn, V. Florescu et al., “Compton scattering revisited,” Radiation Physics and Chemistry vol. 79,2, pp. 124-131, 2010.

[81] M. Cooper, P. Mijnarends, N. Shiotani et al., X-ray Compton scattering: OUP Oxford, 2004.

[82] F. Aharonian, A. J. A. Atoyan, and S. Science, “Compton scattering of relativistic electrons in compact X-ray sources,” Astrophysics and Space Science vol. 79,2, pp. 321-336, 1981.

[83] F. Van der Veen, and F. J. J. o. P. C. M. Pfeiffer, “Coherent x-ray scattering,” vol. 16,28, pp. 5003, 2004.

[84] B. J. N. Lengeler, “Coherence in X-ray physics,” Naturwissenschaften vol. 88,6, pp. 249-260, 2001.

[85] D. Joshi, and T. P. J. A. I. R. Singh, “A survey of fracture detection techniques in bone X-ray images,” Artificial Intelligence Review vol. 53,6, pp. 4475-4517, 2020.

[86] F. Hardalaç, F. Uysal, O. Peker et al., “Fracture detection in wrist X-ray images using deep learning-based object detection models,” vol. 22,3, pp. 1285, 2022.

[87]P Simoni, “Optimisation of X-Rays Imaging Techniques for the Assessment of Joint Space,” J Belg Soc Radiol vol. 102,1, pp. 23, 2018.

[88] C. Spampinato, S. Palazzo, D. Giordano et al., “Deep learning for automated skeletal bone age assessment in X-ray images,” Med Image Anal vol. 36, pp. 41-51, 2017.

[89] V. De Sanctis, S. Di Maio, A. T. Soliman et al., “Hand X-ray in pediatric endocrinology: Skeletal age assessment and beyond,” Indian J Endocrinol Metab vol. 18, Suppl 1, pp. S63-S71, 2014.

[90] A. Horng, E. Brun, A. Mittone et al., “Cartilage and soft tissue imaging using X-rays: propagation-based phase-contrast computed tomography of the human knee in comparison with clinical imaging techniques and histology,” Invest Radiol vol. 49,9, pp. 627-634, 2014.

[91] S.A. Jebb, “Measurement of soft tissue composition by dual energy X-ray absorptiometry,” Br J Nutr vol. 77,2, pp. 151-163, 1997.

[92] W.R Hendee “History and status of x-ray mammography,” Health Phys vol. 69,5, pp. 636-648, 1995.

[93] V. Rebuffel, J.-M. J. I.-n.-d. t. Dinten, and c. monitoring, “Dual-energy X-ray imaging: benefits and limits,” Insight vol. 49,10, pp. 589-594, 2007.

[94] H. MacMahon, F. Li, R. Engelmann et al., “Dual energy subtraction and temporal subtraction chest radiography,” J Thorac Imaging vol. 23,2, pp. 77-85, 2008.

[95] H. Chen, M. M. Rogalski, and J. N. J. P. C. C. P. Anker, “Advances in functional X-ray imaging techniques and contrast agents,” Phys Chem Chem Phys vol. 14,39, pp. 13469-13486, 2012.

[96] X. Li, N. Anton, G. Zuber et al., “Contrast agents for preclinical targeted X-ray imaging,” Adv Drug Deliv Rev vol. 76, pp. 116-133, 2014.

[97] S. Kositbowornchai, R. Nuansakul, S. Sikram et al.,

"Root fracture detection: a comparison of direct digital radiography with conventional radiography," Dentomaxillofac Radiol vol. 30,2, pp. 106-109, 2001.

[98] L. Yin, A. Basu, and J. K. J. P. R. Chang, "Scalable edge enhancement with automatic optimization for digital radiographic images," Pattern Recognition vol. 37,7, pp. 1407-1422, 2004.

[99] W. Chen, X. Liu, K. Li et al., "A deep-learning model for identifying fresh vertebral compression fractures on digital radiography," Eur Radiol vol. 32,3, pp. 1-10, 2022.

[100] S. Jett, M. K. Shrout, J. M. Mailhot et al., "An evaluation of the origin of trabecular bone patterns using visual and digital image analysis," Oral Surg Oral Med Oral Pathol Oral Radiol Endod vol. 98,5, pp. 598-604, 2004.

[101] A. Meesters, K. Ten Duis, J. Kraeima et al., "The accuracy of gap and step-off measurements in acetabular fracture treatment," Sci Rep vol. 11,1, pp. 18294, 2021.

[102]ML Sampaio, and Reporting, "Fracture Healing and Complications of Fractures," pp. 341-377, 2012.

[103] A. Niiya, K. Murakami, R. Kobayashi et al., "Development of an artificial intelligence-assisted computed tomography diagnosis technology for rib fracture and evaluation of its clinical usefulness," Sci Rep vol. 12,1, pp. 8363, 2022.

[104] M. Miniati, S. Monti, J. Stolk et al., "Value of chest radiography in phenotyping chronic obstructive pulmonary disease," Eur Respir J vol. 31,3, pp. 509-515, 2008.

[105] D. Wootton, and C. J. P. Feldman, "The diagnosis of pneumonia requires a chest radiograph (x-ray)—yes, no or sometimes?," vol. 5,1, pp. 1-7, 2014.

[106] G. E. Hayden, and K. W. J. T. J. o. e. m. Wrenn, "Chest radiograph vs. computed tomography scan in the evaluation for pneumonia," J Emerg Med vol. 36,3, pp. 266-270, 2009.

[107] R. Piccazzo, F. Paparo, and G. J. T. J. o. R. S. Garlaschi, "Diagnostic accuracy of chest radiography for the diagnosis of tuberculosis (TB) and its role in the detection of latent TB infection: a systematic review," J Rheumatol Suppl vol. 91, pp. 32-40, 2014.

[108] M. M. Oken, W. G. Hocking, P. A. Kvale et al., "Screening by chest radiograph and lung cancer mortality: the Prostate, Lung, Colorectal, and Ovarian (PLCO) randomized trial," JAMA vol. 306,17, pp. 1865-1873, 2011.

[109] M. M. Oken, P. M. Marcus, P. Hu et al., "Baseline chest radiograph for lung cancer detection in the randomized Prostate, Lung, Colorectal and Ovarian Cancer Screening Trial," J Natl Cancer Inst vol. 97,24, pp. 1832-1839, 2005.

[110] J. Kim, and K. H. J. T. l. c. r. Kim, "Role of chest radiographs in early lung cancer detection," Transl Lung Cancer Res vol. 9,3, pp. 522, 2020.

[111] J. Gohagan, P. Marcus, R. Fagerstrom et al., "Baseline findings of a randomized feasibility trial of lung cancer screening with spiral CT scan vs chest radiograph: the Lung Screening Study of the National Cancer Institute," Chest vol. 126,1, pp. 114-121, 2004.

[112] Z. Nxumalo, E. Irusen, B. Allwood et al., "The utility of artificial intelligence in identifying radiological evidence of lung cancer and pulmonary tuberculosis in a high-burden tuberculosis setting," S Afr Med J vol. 114,6, pp. 29-31, 2024.

[113] J.C. Wandtke, "Bedside chest radiography," Radiology vol. 190,1, pp. 1-10, 1994.

[114] L. Delrue, R. Gosselin, B. Ilsen et al., "Difficulties in the interpretation of chest radiography," pp. 27-49, 2011.

[115] Z. Szucs-Farkas, A. Schick, J. L. Cullmann et al., "Comparison of dual-energy subtraction and electronic bone suppression combined with computer-aided detection on chest radiographs: effect on human observers' performance in nodule detection," AJR Am J Roentgenol vol. 200,5, pp. 1006-1013, 2013.

[116] J. D. Balkman, S. Mehandru, E. DuPont et al., "Dual energy subtraction digital radiography improves performance of a next generation computer-aided detection program," J Thorac Imaging vol. 25,1, pp. 41-47, 2010.

[117] J. Iannucci, and L. J. Howerton, Dental radiography-E-book: principles and techniques: Elsevier Health Sciences, 2016.

[118] C. W. Douglass, R. W. Valachovic, A. Wijesinha et al., "Clinical efficacy of dental radiography in the detection of dental caries and periodontal diseases," Oral Surg Oral Med Oral Pathol vol. 62,3, pp. 330-339, 1986.

[119] B. E. Angmar-Månsson, S. Al-Khateeb, and S. J. J. o. d. e. Tranæus, "Caries diagnosis," J Dent Educ vol. 62,10, pp. 771-780, 1998.

[120] E. Levander, R. Bajka, and O. J. T. E. J. o. O. Malmgren, "Early radiographic diagnosis of apical root resorption during orthodontic treatment: a study of maxillary incisors," Eur J Orthod vol. 20,1, pp. 57-63, 1998.

[121] H. Crow, E. Parks, J. Campbell et al., "The utility of panoramic radiography in temporomandibular joint assessment," Dentomaxillofac Radiol vol. 34,2, pp. 91-95, 2005.

[122] R. H. Sukhia, R. Nuruddin, S. I. Azam et al., "Predicting the sagittal skeletal pattern using dental cast and facial profile photographs in children aged 9 to 14 years," J

Pak Med Assoc vol. 72,11, pp. 2198-2203, 2022.

[123] R. D. Leathers, and R. E. J. A. O. M. S. C. N. A. Gowans, “Office-based management of dental alveolar trauma,” Atlas Oral Maxillofac Surg Clin North Am vol. 21,2, pp. 185-197, 2013.

[124] J. De Mey, B. O. De Beeck, M. Meysman et al., “Real time CT-fluoroscopy: diagnostic and therapeutic applications,” Eur J Radiol vol. 34,1, pp. 32-40, 2000.

[125] K. Katada, R. Kato, H. Anno et al., “Guidance with real-time CT fluoroscopy: early clinical experience,” Radiology vol. 200,3, pp. 851-856, 1996.

[126] E. Seeram, E. J. D. R. P. P. Seeram, and Q. Control, “Digital fluoroscopy,” pp. 95-110, 2019.

[127] D.J. DiSantis, “Gastrointestinal fluoroscopy: what are we still doing?” vol. 191,5, pp. 1480-1482, 2008.

[128] S. J. Leibovic, and W. J. J. T. B. J. o. R. Caldicott, “Gastrointestinal fluoroscopy: patient dose and methods for its reduction,” Br J Radiol vol. 56,670, pp. 715-719, 1983.

[129] M. S. Levine, P. Ramchandani, and S. E. Rubesin, Practical Fluoroscopy of the GI and GU Tracts: Cambridge University Press, 2012.

[130] V.A Duddalwar, “Multislice CT angiography: a practical guide to CT angiography in vascular imaging and intervention,” Br J Radiol vol. 77, suppl_1, pp. S27-S38, 2004.

[131] R. A. Byrne, S. Cassese, M. Linhardt et al., “Vascular access and closure in coronary angiography and percutaneous intervention,” Nat Rev Cardiol vol. 10,1, pp. 27-40, 2013.

[132] D. Bernardi, P. Macaskill, M. Pellegrini et al., “Breast cancer screening with tomosynthesis (3D mammography) with acquired or synthetic 2D mammography compared with 2D mammography alone (STORM-2): a population-based prospective study,” Lancet Oncol vol. 17,8, pp. 1105-1113, 2016.

[133] M. Elzaki, “Evidence on synthesized two-dimensional mammography versus digital mammography when using tomosynthesis (three-dimensional mammography) for population breast cancer screening,” Clinical Breast Cancer vol. 18,4, pp. 255-260. e251, 2018.

[134] J. M. Lewin, C. J. D'Orsi, R. E. Hendrick et al., “Clinical comparison of full-field digital mammography and screen-film mammography for detection of breast cancer,” AJR Am J Roentgenol vol. 179,3, pp. 671-677, 2002.

[135] S. Batchu, F. Liu, A. Amireh et al., “A review of applications of machine learning in mammography and future challenges,” Oncology vol. 99,8, pp. 483-490, 2021.

[136] M. A. Baysal, and E. Toker, "CMOS cassette for digital upgrade of film-based mammography systems." pp. 615-623.

[137] Y.-H. Hu, M. Masiar, and W. Zhao, "Breast structural noise in digital breast tomosynthesis and its dependence on reconstruction methods." pp. 598-605.

[138] H. R. Peppard, B. E. Nicholson, C. M. Rochman et al., “Digital breast tomosynthesis in the diagnostic setting: indications and clinical applications,” Radiographics vol. 35,4, pp. 975-990, 2015.

[139] H. Wobser, R. Wiest, B. Salzberger et al., “Evaluation of treatment response after chemoembolisation (TACE) in hepatocellular carcinoma using real time image fusion of contrast-enhanced ultrasound (CEUS) and computed tomography (CT)-preliminary results,” Clin Hemorheol Microcirc vol. 57,2, pp. 191-201, 2014.

[140] Y. Yu, M. Guo, X. J. C. b. Han et al., “Comparison of multi-slice computed tomographic angiography and dual-source computed tomographic angiography in resectability evaluation of pancreatic carcinoma,” Cell Biochem Biophys vol. 70,2, pp. 1351-1356, 2014.

[141] K. Nieman, M. Oudkerk, B. J. Rensing et al., “Coronary angiography with multi-slice computed tomography,” Lancet vol. 357,9256, pp. 599-603, 2001.

[142] T. Flohr, B. J. M.-s. Ohnesorge, and D.-s. C. i. C. Imaging, “Multi-slice CT technology,” pp. 41-69, 2007.

[143] M. F. Reiser, C. R. Becker, K. Nikolaou et al., Multislice ct: Springer Science & Business Media, 2008.

[144] B. M. Ohnesorge, Multi-Slice CT in Cardiac Imaging: Technical Principles, Clinical Applications and Future Developments: Springer Science & Business Media, 2002.

[145] A. Inamdar, and R. K. J. C. Shinde, “The diagnostic impact of contrast-enhanced computed tomography (CECT) in evaluating lymph node involvement in colorectal cancer: a comprehensive review,” Cureus vol. 16,6, pp. e61832, 2024.

[146] J. Huang, W. Chen, and S. J. M. Yao, “Assessing diagnostic value of contrast-enhanced ultrasound and contrast-enhanced computed tomography in detecting small hepatocellular carcinoma: A meta-analysis,” Medicine (Baltimore), vol. 96,30, pp. e7555, 2017.

[147] X. Ou, X. Chen, X. Xu et al., “Recent development in x-ray imaging technology: Future and challenges,” Research (Wash D C) vol. 2021, pp. 9892152, 2021.

[148] H. A. Field Jr, "Uses and Limitations of X-Ray Pictures as Evidence." p. 219.

[149] E. L. J. A. i. X.-r. a. Ritman, “Medical x-ray imaging, current status and some future challenges,” vol. 49, pp. 1-

12, 2006.

[150] M. J. Müller, W. Braun, J. Enderle et al., “Beyond BMI: conceptual issues related to overweight and obese patients,” vol. 9,3, pp. 193-205, 2016.

[151] M. J. Modica, K. M. Kanal, and M. L. J. R. Gunn, “The obese emergency patient: imaging challenges and solutions,” Radiographics vol. 31,3, pp. 811-823, 2011.

[152] M. S. Lopes, P. P. Freitas, M. C. Carvalho et al., “Challenges for obesity management in a unified health system: the view of health professionals,” Fam Pract vol. 38,1, pp. 4-10, 2021.

[153] L. T. Niklason, B. T. Christian, L. E. Niklason et al., “Digital tomosynthesis in breast imaging,” Radiology vol. 205,2, pp. 399-406, 1997.

[154] J. T. Dobbins III, H. P. McAdams, D. J. Godfrey et al., “Digital tomosynthesis of the chest,” vol. 23,2, pp. 86-92, 2008.

[155] P. C. Bunch, K. E. Huff, and R. J. J. o. t. O. S. o. A. A. Van Metter, “Analysis of the detective quantum efficiency of a radiographic screen–film combination,” vol. 4,5, pp. 902-909, 1987.

[156] R. M. Nishikawa, and M. J. J. M. p. Yaffe, “Effect of various noise sources on the detective quantum efficiency of phosphor screens,” Medical Physics vol. 17,5, pp. 887-893, 1990.

[157] P. C. Bunch, "Detective quantum efficiency of selected mammographic screen-film combinations." pp. 67-77.

[158] W.T. Drost, “Transitioning to digital radiography,” J Vet Emerg Crit Care (San Antonio), vol. 21,2, pp. 137-143, 2011.

[159] M. Cellina, M. Cè, G. Irmici et al., “Artificial intelligence in emergency radiology: where are we going?” Diagnostics (Basel), vol. 12,12, pp. 3223, 2022.

[160] A. Kalyanpur, and N. J. A. M. Mathur, “Applications of artificial intelligence in thoracic imaging: a review,” vol. 2,1, 2025.

[161] G. Kalifa, Y. Charpak, C. Maccia et al., “Evaluation of a new low-dose digital x-ray device: first dosimetric and clinical results in children,” Pediatr Radiol vol. 28,7, pp. 557-561, 1998.

[162] T. Hugh, Morgan, “Dose reduction for CT pediatric imaging,” Pediatr Radiol vol. 32,10, pp. 724-728; discussion 751-724, 2002.

[163] E. H. Silver, S. D. Shulman, and M. M. J. M. P. Rehani, “Innovative monochromatic x-ray source for high-quality and low-dose medical imaging,” Med Phys vol. 48,3, pp. 1064-1078, 2021.

[164] J. Wong, P. Kutschera, and K. K. J. J. o. c. a. t. Lau, “Spectral Shaping Computed Tomography Applications,” pp. 10.1097, 2022.

[165] S. Rajsic, R. Breitkopf, M. Bachler et al., “Diagnostic modalities in critical care: point-of-care approach,” Diagnostics (Basel), vol. 11,12, pp. 2202, 2021.

[166 M. Di Serafino, G. Dell’Aversano Orabona, M. Caruso et al., “Point-of-Care Lung Ultrasound in the Intensive Care Unit—The Dark Side of Radiology: Where Do We Stand?,” vol. 13,11, pp. 1541, 2023.

[167] D. Gutierrez, S. Schmidt, A. Denys et al., “CT-automatic exposure control devices: What are their performances?”, vol. 580,2, pp. 990-995, 2007.

[168] Y. E. Almalki, A. Qayyum, M. Irfan et al., "A novel method for COVID-19 diagnosis using artificial intelligence in chest X-ray images." p. 522.

[169] S. S. Hsieh, S. Leng, K. Rajendran et al., “Photon counting CT: clinical applications and future developments,” IEEE Trans Radiat Plasma Med Sci vol. 5,4, pp. 441-452, 2020.

[170] A. Meloni, F. Frijia, D. Panetta et al., “Photon-counting computed tomography (PCCT): technical background and cardio-vascular applications,” Diagnostics (Basel), vol. 13,4, pp. 645, 2023.

[171] A. C. Alves, A. Ferreira, G. Luijten et al., “Deep PCCT: Photon Counting Computed Tomography Deep Learning Applications Review,” 2024.

[172] M. C. Zdora, “State of the Art of X-ray Speckle-Based Phase-Contrast and Dark-Field Imaging,” Journal of Imaging vol. 4,5, pp. 60, 2018.

[173] F. Pfeiffer, M. Bech, O. Bunk et al., “X-ray dark-field and phase-contrast imaging using a grating interferometer,” Journal of Applied Physics vol. 105,10, 2009.

[174] T. Thüring, R. Guggenberger, H. Alkadhi et al., “Human hand radiography using X-ray differential phase contrast combined with dark-field imaging,” vol. 42,6, pp. 827-835, 2013.

[175] S. J. Hoffman, A. H. Yee, J. P. Slusser et al., “Neuroimaging patterns of ischemic stroke after percutaneous coronary intervention,” Catheter Cardiovasc Interv vol. 85,6, pp. 1033-1040, 2015.

[176] M.-C. J. J. o. I. Zdora, “State of the art of X-ray speckle-based phase-contrast and dark-field imaging,” Journal of Imaging vol. 4,5, pp. 60, 2018.

[177] T. Thüring, R. Guggenberger, H. Alkadhi et al., Human hand radiography using X-ray differential phase contrast combined with dark-field imaging, 0364-2348, Springer, 2013.

[178] S. L. Brady, A. T. Trout, E. Somasundaram et al., "Improving image quality and reducing radiation dose for pediatric CT by using deep learning reconstruction," Radiology vol. 298,1, pp. 180-188, 2021.

[179] C. Catalano, M. Francone, A. Ascarelli et al., "Optimizing radiation dose and image quality," Eur Radiol vol. 17, Suppl 6, pp. 26-32, 2007.

Journal of sustainable food, water, energy and environment

A review of grid connection performance of solar cells for a three-phase structure of a 7-level cascaded inverter

Ahmed M. Montaser[1], Rofida T. Madani[1], Shazly A. Mohamed[2], Rasha Kassem[1]

[1]Electrical Department, Faculty of Technology and Education, Sohag University, Sohag 82524, Egypt
[2]Department of Electrical Engineering, Faculty of Engineering, South Valley University, Qena 83523, Egypt

Received: 2 Aug. 2025, Revised: 20 Sep. 2025, Accepted: 22 Sep. 2025 Published online: 28 Sep. 2025

Abstract: Nowadays, solar energy has become a competitive option for power generation in self-sufficient systems that may be used in both urban and rural electrification settings. High-quality alternating current output is required from the power electronic converters used in the conversion process in order to guarantee a voltage waveform that closely mimics a sinusoidal form. To get a high-quality output, the inverter's architecture and the pulse width modulation (PWM) technology it uses are essential factors. With a wide variety of industrial applications, the multilevel inverter has emerged as a major field of study in recent decades. Multilevel inverters (MLIs) are used to enhance output waveform characteristics (e.g., lower total harmonic distortion) and to offer a variety of inverter configurations and modulation methods. As a result, MLIs have attracted more attention from scholars in comparison to their two-level equivalents, attributable to their capacity to deliver reduced electromagnetic interference (EMI), enhanced efficiency, and elevated direct current connection voltages. The Cascaded H-bridge (CHB) inverter was discovered in fact more reliable, easier to build, and performing Impressively among many multilevel inverter configurations. It is the best option for energy transformation in a wide range of industrial applications because of its exceptional qualities, which include great adaptability and durability against defects. This operating efficiency for a three-phase, 7-level CHB inverter was thoroughly investigated at this work. Phase Shifted Pulse Width Modulation (PSPWM) methodology was employed at simulation to assess inverter performance. The three-phase, 7-level CHB inverter was the particular application for this PSPWM technology. MATLAB/SIMULINK software was employed at produce simulator conclusions. The thorough simulation and performance evaluation of a three-phase, seven-level CHB Multilevel Inverter using PSPWM in compliance with real-world operating conditions is what makes this work unique. As opposed to previous studies that primarily focus on generic CHB inverter designs, this paper carefully examines the complex application and performance metrics of PSPWM in a multi-phase system, clarifying issues regarding harmonic distortion properties, voltage waveform integrity, and modulation effectiveness. The suggested inverter is perfect for integration with renewable energy grids because simulations showed that it had better output waveform, reduced power losses, lower harmonic distortions, and superior voltage quality.

Keywords: Multilevel inverters (MLIs); electromagnetic interference (EMI); Cascaded H-bridge (CHB); Phase Shifted Pulse Width Modulation (PSPWM)

Abbriviations:

- MLIs Multilevel inverters
- EMI electromagnetic interference
- CHB Cascaded H-bridge
- PSPWM Phase-Shifted Pulse width modulation
- PV Photovoltaic
- THD Total harmonic distortion
- NPC Neutral Point Clamped
- FC Flying Capacitor
- MPPT Maximum power point tracking
- THD Total harmonic distortion
- SHEPWM Selective Harmonic
- Elimination PWM
- SVPWM Space Vector PWM
- P&O Perturbation and Observation
- IC Incremental Conductance
- SM submodules
- PLL Phase-Locked Loop

1.Introduction

The use of grid-supplied electricity has significantly increased recently. These phenomena can be attributed to the expansion of high-energy sectors and an expanding user demography. Traditional energy production It brought about notable rise at worldwide emissions, which has had negative environmental effects. Significant progress has been made in integrating renewable energy sources, such wind and solar, into the electrical system. Welcome to the world of photovoltaic (PV) systems, which, because of their exceptional potential, have become the best choice for

* Corresponding author E-mail: rofidatm@gmail.com
Print ISSN 3062-5513 Online ISSN 3062-5521

energy capture. In actuality, grid-connected solar PV's capacity has increased to over 635 GW globally, meeting around 2% of the world's energy needs [1].

The solar photovoltaic (PV) technology has the unique benefit of directly converting solar radiation into electrical energy, which makes it especially suitable for a wide variety for geographic locations. As like, it is significantly preferred when compared to other renewable energy sources (RES). In particular, solar power is distinguished by its lack of pollution, its availability due to sun radiation, and its steadily rising prices over the previous 20 years [2]. An important factor in the planet's total energy dynamics is solar radiation. More than 100,000 terawatts for overall quantity from sun rays that solar emits make it through the Earth's atmosphere through processes of absorption and reflection. This enormous store of wasted power having capacity that establish sun power as key component of the renewable energy spectrum [3]. Out of all the photovoltaic systems, over 99 percent are either autonomous or integrated into the electricity grid. This supremacy can be ascribed to lower building costs, increased scalability, shorter downtime, and greater stability of grid-connected networks over their independent counterparts in terms of future growth. [4]. The development of photovoltaic power converters has unquestionably been accelerated by this proliferation. When attaching photovoltaic modules at alternating current (AC) loads as well as electrical network, these converters are quite important. They are therefore used ensuring dependable as well effective power transformation. This basic operations from Photovoltaic energy transformers are always the same, despite the fact that their designs can vary. MLIs had been that most common technology in the industrial sector in recent years because of their remarkable features. They're extensively utilized into network-connected PV power generation systems in medium-for high-power settings [5].

MLIs you class from energy electronic converters which can generate a given alternating waveform with several steps, depending on the number of levels and modulation method used. Due to their use in medium voltage drive applications, which typically have power and voltage ratings between 1 MW and 4 MW and between 3.3 kV and 6.6 kV, respectively, these inverters are well-known. Moreover, the ability of multilevel inverters to produce a staircase waveform that closely resembles a pure sinusoidal waveform with negligible harmonic distortion sets them apart. Depending above required number from sources, MLIs can be divided into two different types: single DC supply inverters as well multiple DC supply inverters [6]. Modular Multilevel Inverters (MLIs) are the recommended choice for integrating with medium voltage power grids because 2-Level inverters are inappropriate for medium voltage applications due to the restrictions imposed by the blocking voltage of semiconductors. In order to meet established grid codes, the MLI not only lessens the dv/dt stress that semiconductor switches face, but it also drastically lowers the voltage Total Harmonic Distortion (THD). Additionally, it has been shown that they can reduce electromagnetic interference (EMI) and power dissipation in semiconductor switches. According to their architecture, MLIs have typically separated into three main topologies: Flying Capacitor (FC), CHB, and Neutral Point Clamped (NPC) [7].

The CHB-MLI is thought to be the best topology of the ones discussed above for integrating a PV system. For every bridge, the CHBMLI includes a separate direct current (DC) supply. The DC sources can be efficiently replaced with a solar panel. Because it has fewer components and allows for the use of an asymmetrical DC source, the CHBMLI has clear advantages over the other two types of MLIs. This output voltage produced by an CHBMLI is twice that of its diode-clamped and flying capacitor equivalents while keeping the input voltage constant [8].

In this paper, design as well modeling from a Three phase 7- level CHB-MLI is discussed of PSPWM technique. This paper also presents a brief overview of modulation technique. Simulation results of output voltage waveforms obtained for Three phase 7- level CHB-MLI are presented using modification technique.

This organization of this paper is as enumerated. Following the introduction in Section 1, Section 2 presents the system General Description in this study. Section 3 presents the topology description. Section 4 presents the main controller. Section 5 provides the simulation outcomes. Section 6 provides the general conclusion as well abbreviations.

Three common types of MLIs are compared in Table 1: (FC-MLI), (NPC-MLI), and (CHB-MLI). This comparison analysis clarifies the essential technological differences that have a substantial impact on each inverter category's operational effectiveness, providing important information about their suitability for various applications. This comparison led to the selection of CHB due to its fault tolerance, modularity, high efficiency, low harmonic distortion, and applicability in solar PV applications with independent DC sources.

2. General Description

Figure 1 shows a three-phase 7-level CHB-MLI system with PV systems which is connected for electrical network and Modulation technique was used. This topology indicates to how the component arrangement and functionality by implementing the following methods: -

- The PV module converts solar energy, which is defined as solar radiation for 1000 W/m² and degree from 25°C into electrical energy in the form of current as well voltage signals.

Table 1: CHB, NPC and FC multilevel inverter comparison.

	CHB-MLI	NPC-MLI	FC-MLI	Ref
Response Speed	Depending on the PWM being utilized (like APOD, PSPWM, etc), the response time is medium.	Similar, but balance makes control more difficult.	Similar, but because there are more capacitors, the control is more complicated.	[9 - 10]
Losses	Reduced stress on the keys and low losses because there aren't several capacitors.	Increased losses because of capacitors used for voltage stabilization.	Losses increase as complexity and capacitor count rise.	[3,9,11]
THD	The low total harmonic distortion is a result of the independent operation of each H-bridge, allowing for modulation that produces an output waveform closely resembling a sinusoidal shape. This modular design improves harmonic performance.	Multiple voltage levels help to reduce the number of steps in the output waveform, which in turn helps to achieve a low total harmonic distortion. However, careful capacitor voltage balancing is required to achieve a moderate THD.	THD is often modest and comparable to NPC. The output waveform can be fine-tuned thanks to the voltage level flexibility, which lowers THD. However, the capacitor voltage balancing affects the THD.	[11- 12]
Efficiency	Reduced component stress and the ability to distribute power conversion over multiple modules are responsible for increased efficiency, particularly at higher power levels. (97–99%).	Due to lower switching losses, especially at lower switching frequencies, the efficiency is typically higher. Nevertheless, when the number of levels increases, the total efficiency decreases because of the additional power losses brought on by the clamping diodes. (96–98%).	usually reduced relative to the nominal power consumption due to additional energy loss associated with the charging and discharging of the capacitors. In order to maintain operational efficiency (94–97%), careful monitoring of capacitor voltages is required.	[9, 12 - 13]
Complexity Structural	Low; symmetrical cells and distinct structure H-Bridge	Medium to high (voltage stabilizer and several capacitors).	Very high (difficult to balance and too many capacitors).	[3, 11, 14, 35]
Scalability	Extremely high; increasing the number of cells to level up is simple.	Restricted; as levels rise the design gets more intricate.	Restricted; as levels rise the design gets more intricate.	[14, 35]
Cost	Reasonably low for systems with independent DC sources; particularly for modular applications.	high because of the extra ingredients.	extremely intricate and high in capacitors accumulation.	[3, 11, 35]
Fault Tolerance	Excellent; operation can continue at lesser levels and a failed cell can be circumvented.	weak	Medium (but FC allows for the usage of double cases).	[14, 35]
Applications	Widespread use is seen in medium- to high-voltage drive systems, electric vehicles, Flexible AC Transmission System (FACTS) devices, and renewable energy domains (such solar inverters and wind turbines).	frequently used in medium-voltage driving applications, Static Synchronous Compensators (STATCOMs), High Voltage Direct Current (HVDC) systems, and electrical power transmission frameworks.	Suitable for applications requiring high levels of redundancy and adaptability, such as high-voltage medical equipment and aerospace systems.	[12]

- A MPPT controller system controlled by genetic algorithms is used to monitor these signals, guaranteeing their constancy to maximize power output.
- The Boost Converter receives the constant voltage and current signals and raises the output terminal's voltage.
- A CHB seven-level inverter utilizing their Sinusoidal PWM technology is used to convert the maximum output voltage signals into alternating current voltage signals by
- comparing the reference and carrier signals.
- Additionally, sinusoidal alternating current voltage signals are produced and then filtered by alternating current filter circuits to eliminate unnecessary signals, which helps to fewer THD.

This modulation technique, an PWM circuit was utilizes generating impulses for CHB inverter. Several PWM methods, like multi-carrier PWM, Selective Harmonic Elimination PWM (SHEPWM), as well Space Vector PWM (SVPWM), are utilized to reduce harmonics in the inverter's output, which results in a more refined alternating current waveform. Harmonic distortion reduction is necessary for the reliable integration of the inverter with the main electrical grid.

2.1 Topology Description

A. Cascaded H-Bridge

Figure 2 shows a solar energy conversion system that uses the MPPT algorithm to get better the competence for energy extraction from PV panels. PV panels provide the system's initial direct current power, which is then converted by a boost converter to provide a higher DC voltage. In order to maintain optimal power output in the face of changing external conditions, the MPPT controller continuously monitors the voltage V_{PV} and current I_{PV} generated by the solar panels.

Two or more single-phase inverters have linked for series to formation CHB-MLI, which is why it is called a "H-bridge." This is the inverter's output voltage represented by line-to-line, and Everyone H-bridge is connected to two phase legs of voltage-source. As a result, an H-bridge converter could produce three various voltage levels. Moreover, the N of these H-bridges connected in series can produce a total of 2N+1 output voltage levels. This CHB-MLI was the name gave to this arrangement of series connectivity [15].

When this specific kind of inverter operates, it usually produces three different outputs: Vdc, 0Vdc, and -Vdc. Switches S1 and S4 must be engaged in order to produce a Vdc output, while switches S2 and S3 must be engaged in order to produce a -Vdc output. According to equation (1), the total of all the individual H-bridges is output voltage for CHB-MLI. This formula n = 2S + 1, wherever S is total numeral of DC sources, can be used to quantify the levels generated by this inverter setup [16]: -

$$V_a = V_1 + V_2 + V_3 + V_4 \qquad (1)$$

The main benefits and drawbacks of the traditional (CHB-MLI) architecture are listed in Table 2 [3,17-20]. The chart highlights its inherent fault-tolerance, modular design, and ease of implementation as key advantages. On the other hand, it also highlights several drawbacks, such as the need for many separate DC power sources and the complex control systems required for asymmetrical arrangements.

It has been explained that the advantages of (CHB-MLI) include fewer parts, a simpler design, and an easy-to-use switching mechanism. It is easy to adjust this inverter's output voltage by increasing or decreasing that numeral of H-bridges. Since n = 2S + 1 determines that output voltage levels, this leads to values that are much higher than those obtained from a direct current source. As a result, this specific inverter creates production operation additional transparent as well economical. For conclusion, the CHB-MLI performs best Regarding dependability as well ideal error resilience capacities than Neutral Point Clamped MLI and Flying Capacitor MLI. Because of these benefits, the inverter can function more effectively when the DC input voltage is lower [16].

The uses for CHBMLI are [18, 21]: -

- This CHBMLI is suitable for large energy average voltage engines as well Facilities uses.
- crossbred electrical as well Fuel cell engines.
- Traction engines.
- Flexible alternating current transmission system.
- PV energy production.
- In constant Var generators.
- Power factor compensators.

B. Principles of Operation

The schematic design of the DC-DC boost converter used in the suggested framework is shown in Figure 3. The inductor L, input and output capacitors C_{in} and C_{out}, the switching device S, and the diodes D_1 and D_2 are among its necessary parts. In order to accommodate the load R, this type of converter is used to raise the input voltage V_I to a higher output voltage V_O, which makes it especially useful for solar energy applications that require higher power conversion competence.

The grid-tied H-bridge inverter system effectively transforms solar energy into alternating current electricity that is compatible with the electrical grid by combining a photovoltaic cell, a boost DC/DC converter, and (MPPT) technique. Direct current power generation from solar radiation is facilitated by the photovoltaic cell. To ensure that the solar cell runs at its maximum power output even when external conditions fluctuate, a MPPT approach must be used.

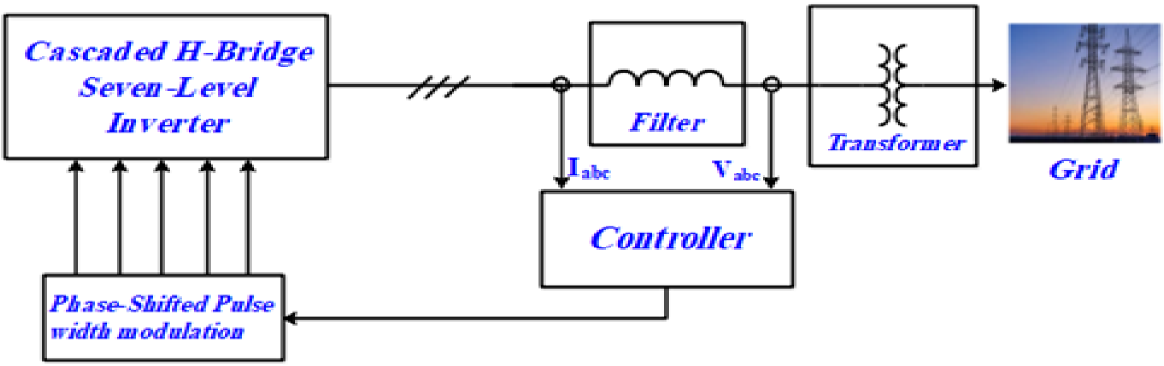

Fig. 1: Grid-Connected CHB Inverter System

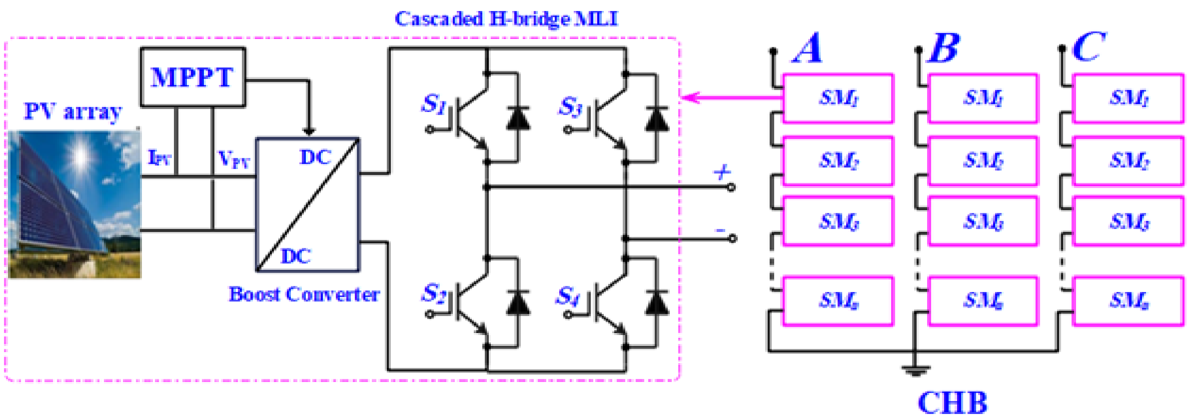

Fig. 2: Solar Power Conversion System with MPPT and CHB MLI

Table 2: Benefits and drawbacks for traditional topology CHB-MLI

Types of MLI	Benefits	drawbacks
CHB-MLI	• Simple as well modular design. • Facile into stretch for greater levels. • Demands just one-way switches. • Suitable for error-resistance application. • Possible of electric trauma is decreased due their discrete DC sources. • Asymmetrical exporter structure May be utilized. • May be executed as an one DC source structure.	• Fewer numeral of output voltage tiers. • Demands greater numeral of gateway operator circuits. • Demands sundry DC sources to increment that output voltage. • Restricted to specific applications wherever discrete DC sources were given. • Keys must carry preventing voltage equivalent to the income voltage worth. • Modularity lost (asymmetrical source structure). • Execute expense is large (asymmetrical source structure). • Keys are various voltage rankings (asymmetrical source structure).

The MPPT algorithm continuously adjusts the reference voltage or current parameters to maximize the power collected from the solar cell. The voltage thresholds required for the best possible integration into the electrical grid are usually not met by the direct current voltage generated by solar cells. To address this problem, a step-up DC/DC energy converter, as well recognized like a boost converter, is utilized to raise the DC voltage to a level that is compatible with the H-bridge inverter's operating specifications. The voltage increase ensures that the energy supplied to that H-bridge inverter meets that required input specifications, allowing for an effective conversion to alternating current power. The high voltage direct current output provided by the boost converter is changed into alternating current power by the H-bridge inverter, enabling compatibility with the power grid. The inverter is made of four electronic switching devices organized in an H-bridge arrangement. By adjusting these switches in different ways, the inverter may generate both positive and negative voltage levels, which results in an alternating current waveform. This method facilitates smooth integration with the grid system by guaranteeing that the alternating current output maintains high quality and complies with the grid's voltage, frequency, and phase specifications.

The initial stages of integrating renewable energy sources into a direct current grid are when DC–DC converters are most commonly used. It is crucial that this phase runs as efficiently as possible because RES, such wind and solar photovoltaic systems, are known to cause output voltage swings. Therefore, for the DC–DC converters in the front-end stages to operate as efficiently as possible, they must exhibit a high degree of responsiveness to such fluctuations. They inverters is frequently utilized in tiny industrial or Facilities settings due to higher voltage pressure, subpar competence, high working temperatures, and improved pressure capabilities. Because of their advantageous characteristics, many inverters are commonly utilized big, higher-energy, grid-connected replenishable power systems [1].

The output direct current voltage produced by this converter is higher than the input direct current voltage. As a result, this converter is frequently called a step-up or boost converter. That is made up of one energy storage component, an inductor, and two power electronic switches, a diode as well a metal-oxide-semiconductor field-effect transistor (MOSFET). To lessen that output voltage ripple in this situation, a capacitor is used as a filtering method. In comparison to the transformer less high-gain boost converter, the multilayer boost converter has been suggested to achieve reduced voltage stress and increased efficiency. The direct current to direct current boost converter's linked inductor has been used to generate higher voltage gain and efficiency that are suited to the particular needs of solar power applications [22].

2.2 Main Controller

A. Maximum Power Point Tracking

An integral part of solar (PV) technology's operating framework is monitoring the system's Maximum Power Point. However, the goal of precise tracking is significantly complicated by changing environmental factors, such as temperature and solar light. Numerous MPP tracking techniques been put out as well recorded at scholarly works. Despite optimal power extraction is the goal of all approaches, there are differences among them in terms of complexity, rate of convergence, regulating variables, settling time, required number of sensors, and total cost. Incremental Conductance (IC) as well Perturbation and Observation (P & O) are the most commonly used MPPT techniques in most commercially available inverters and in many academic publications [23].

Observe and Perturb (MPPT Technique) This approach is among the most widely used and conventional (MPPT) strategies used to maximize peak power extraction from solar energy systems. It is distinguished by a small temporal ratio deviation and an operating voltage change that depends on the difference between the power measured in the previous interval and the power measured in the present [22, 24]. By tailoring sample intervals to the dynamic behavior of its converters, the P & O MPPT technique can be made more effective. Using the P&O algorithm, an MPPT shipment controller over 200W standalone PV systems was created. The designed model was tested with a lead-acid battery, showing that the suggested algorithm significantly improves the solar PV model's performance in comparison to other charge controllers currently in use [25].

The flowchart for the improved (P&O) technique is shown in Figure 4. The process begins with the solar panel's voltage and current data being collected, which is followed by the calculation of power and its variations. A decision is made to increase or decrease the duty cycle to precisely follow the MPPT based on the voltage and power changes that have been noticed. This improved method reduces oscillatory around the ideal operating point and greatly improves tracking performance.

A comparison of the efficiency, complexity, cost, and THD of several MPPT control strategies is shown in Table 3. The P&O method is one of the most popular since it is easy to use, inexpensive, and sophisticated, yet it still achieves a respectable efficiency of about 97.6%. Because of this, it is a good choice for systems that need conventional and affordable solutions.

B. Control of Cascaded H-Bridge

The control mechanism used for a MLI design with a CHB for grid integration is schematically represented in Figure 5. SM-A1, SM-A2,... SM-An, SM-B1, SM-B2,... SM-Bn, and SM-C1, SM-C2,... SM-Cn are some of the submodules (SM) that make up the CHB.

Table 3: A comparison of the various MPPT control methods.

MPPT	THD	Efficiency	Complexity	Cost	Ref
P&O	Low (traditional)	~ 97.6%	Simple - medium	Low	[26]
INC	Low	~ 98.5%	average - High	average - High	[26]
FLC	Low (Better response)	very high ~ 99%	High	Very High	[27]
Hybrid	Low	very high ~ 100%	Very High	Very High	[27]

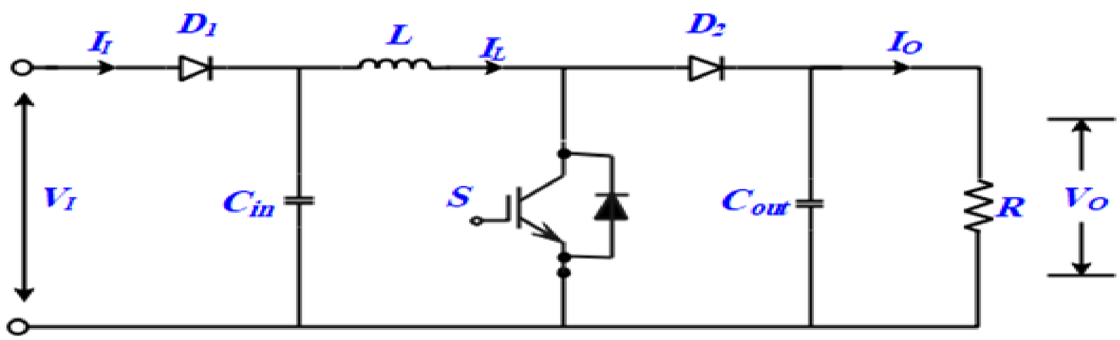

Fig. 3: DC-DC boost converter

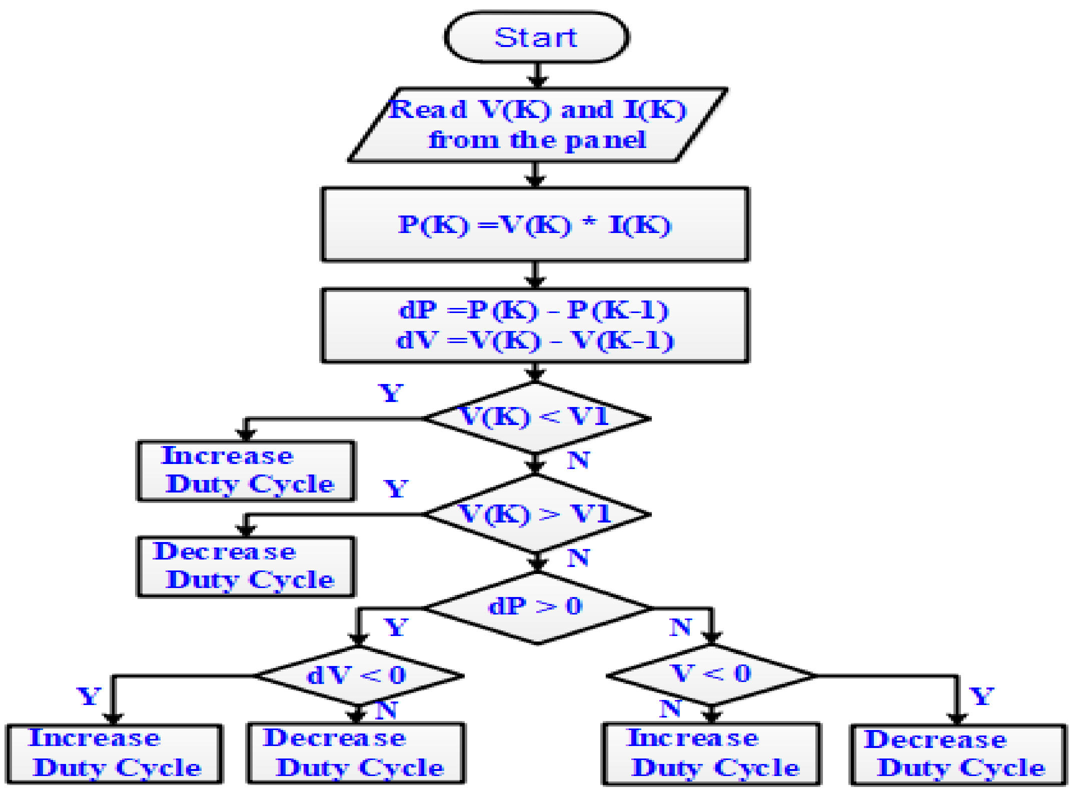

Fig. 4: Flowchart of the modified P&O technique

These submodules together generate the output voltage in a stepped waveform, which makes it easier to achieve high power quality. To synchronize the inverter with the grid's frequency, these submodules are connected to the electrical grid through a Phase-Locked Loop (PLL) as well filtering component known like L_f. order to facilitate their conversion into the dq0 reference frame for the execution of the control strategy, the PLL is in charge of continuously monitoring the grid voltage V_{abc} and the current I_{abc}.

A Proportional-Integral (PI) controller that uses the instantaneous references i_d and i_q to control the DC-link voltage V_{dcm} and manage active and reactive power is one of the several parts of the control system. The dq0 transformation block transforms the grid side currents I_{abc} and voltages V_{abc} into their respective dq components. These dq components are then adjusted by the Proportional-Integral controllers to generate necessary referring voltages, V_d and V_q. These generated reference values are then converted back into the ABC frame and integrated into the modulation phase shift block, which generates the crucial control signals for the CHB submodules, to guarantee optimal synchronization and power quality during the energy injection into the grid.

C. Modulation Technique

CHB inverters commonly use PSPWM technology because of its ease of use and ability to be implemented successfully at different inverter architectural levels. The ability of this technology to provide consistent power distribution among the individual H-Bridge cells inside the inverter system is another notable feature. The amplitude and frequency characteristics of each carrier signal must be equal for Phase Shifted Modulation to be implemented.

In an N-level inverter, however, the required number of carrier waves is N-1, which need to be phase-shifted by an angle

$\frac{360^{\circ}}{N-1}$ relative to each other [6].

When compared to other modulation techniques, the PS-PWM technique has several benefits, such as reduced THD, improved effective switching frequency, balanced power distribution, and optimized semiconductor stress profiles.

In phase-shifted modulation, a (180°⁄N) phase displacement is required when N cells are present in CHB multilevel converters. On the other hand, an (360°⁄N) phase displacement is required for the N cell design in flying capacitor multilevel converters [8].

There is intrinsic flexibility in the frequencies and amplitudes of the sinusoidal modulating signals. In this approach, the amplitude modulation index, or (m_a), makes it easier command that essential -frequency constituent of output voltage from the inverter. The formula ($m_a=V_m/V_{cr}$), in which V_m and V_{cr} represent the peak levels of the modulating and carrier voltage signals, respectively, is used to calculate this index. Phase-shifted carrier signals are combined with modulating signals to provide gateway signals to energy keys. Whenever modification signal was larger than transporter signal, that hybrid boost converters' upper and lower switches are activated [14].

A comparison of different PWM techniques is shown in Table 4, where the PS-PWM method stands out due to its exceptionally low THD of 1% to 4%, remarkable operational efficiency of up to 96%, ease of implementation, and significantly lower cost when compared to other approaches.

PSPWM was selected based on this comparison because it lowers THD, Programming and implementation are simple, distributes losses over all H-bridges in a good way, with many levels, it is scalable and increases efficiency, making it appropriate for applications that demand great performance at a reasonable cost.Although it is not always the best option, PSPWM in a CHB is great for its ease of use, scalability, and implementation that is not affected by distortion or efficiency[34].

Table 5. lists the factors and conditions that are relevant to the simulation, including the switching frequency, load arrangement, photovoltaic panel specs, battery charging parameters, and the time intervals for sampling. These parameters were methodically set up to enable accurate modeling and reliable system performance evaluation.

Table 4: Comparison of PWM techniques' performance

Modulation	THD (%)	Efficiency	Complexity	Cost	Ref
SVPWM	3.5% - 5%	94% - 96%	Average - High	low	[28 -29]
PS-PWM	Low (1 – 4) %	High ~ 96%	low	very low	[14, 29]
NLM	5% - 7%	90% - 93%	High	Average	[29- 31]
SVM	3.8% - 5.2%	94% - 96%	High	Average	[14, 29]
SHE-PWM	1.5% - 3%	95% - 97%	High	High	[32] - [33]

Table 5: shows simulation parameters and conditions.

Parameter Category	Parameter	Value	Unit
Switching Frequency	PWM Switching Frequency MPPT Duty Cycle Step Size	1000 1e-6	Hz -
Load Type	Load Configuration Load Type Active Power (P) Inductive Reactive Power (QL) Capacitive Reactive Power (Qc)	Y (Grounded) Three-Phase Parallel RLC 1000 400 ~ 400	- - W Var Var
PV Panel Specifications	Parallel Strings Series-Connected Modules per String Max Power per Module Open Circuit Voltage (Voc) Short-Circuit Current (Isc) Voltage at Max Power Point (Vmp) Current at Max Power Point (Imp) Series Resistance (Rs) Shunt Resistance (Rsh)	2 4 250.29 36.6 8.75 30.9 8.1 0.12527 126.1585	- - W V A V A Ω Ω
Battery Settings	Battery Charging Constant Voltage	55.4	V
Sampling Time	Power System Sample Time (Ts) Control System Sample Time (Ts_Control)	1e-5 2e-5	seconds (10 µs) seconds (20 µs)

Table 6.: Shows THD analysis before and after filter

Parameter	Before Filtering	After Filtering	Difference (Improvement)
Vabc THD (%)	1.802 V	1.042 V	0.760 V (Improved)
Iabc THD (%)	1.008 A	0.6717 A	0.3363 A (Improved)

3. Conclusions

According to the results, the suggested seven-level CHB-MLI demonstrated outstanding performance by lowering voltage stress, minimizing EMI, reducing harmonic distortion, and enabling fair power distribution among inverter cells. Additionally, the application of a customized MPPT strategy increased the PV system's efficiency. This study offers a comprehensive simulation-based analysis of a three-phase, seven-level CHB-MLI using PSPWM under realistic operating conditions, in contrast to previous studies that mostly concentrated on generic CHB architecture or isolated components like harmonic mitigation or modulation techniques. These findings demonstrate the uniqueness of this study in providing an integrated simulation and performance evaluation that has not been thoroughly covered in previous research, in addition to confirming the reliability of CHB-MLI for the integration of RES.

Contributions of the Authors

The main contributions of this study might be stated as follows considering the findings:

1.Creation of a Customized CHB-MLI for Grid-Based PV Systems:

A CHB-MLI system has been carefully planned and implemented to meet the requirements of grid-connected solar systems, with an emphasis on increasing efficiency and reducing energy losses.

2. Implementing a Customized MPPT Algorithm for Three-Phase Solar Power Systems:

To maximize the energy extraction from PV arrays in a three-phase setting and increase the system's overall effectiveness, a customized MPPT management method has been developed and put into practice.

3.Independent Voltage Regulation Across Multiple DC Sources:

To improve system reliability and voltage stability, a complex control strategy has been put in place to enable independent voltage regulation across the different direct current links of the CHB-MLI.

4.Phase-Shifted PWM Technique:

To ensure fair power distribution among the inverter cells, reduce EMI, and attenuate harmonic distortion, the PSPWM technique has been used.

5.Thorough Analysis of CHB-MLI for Renewable Energy Applications:

The study presents a thorough analysis of the potential uses and capabilities of CHB MLIs in renewable energy systems, clarifying their adaptability and effectiveness in these settings.

5.References

[1] S. Nyamathulla and D. Chittathuru, "A Review of Multilevel Inverter Topologies for Grid-Connected Sustainable Solar Photovoltaic Systems," Sustain., vol. 15, no. 18, 2023, doi: 10.3390/su151813376.

[2] C. Gnanavel and K. Vanchinathan, "Review and design of modular multilevel inverter with modified multicarrier PWM techniques for solar PV applications," Circuit World, vol. 49, no. 4, pp. 528–559, 2023, doi: 10.1108/CW-06-2021-0162.

[3] A. Bughneda, M. Salem, A. Richelli, D. Ishak, and S. Alatai, "Review of multilevel inverters for PV energy system applications," Energies, vol. 14, no. 6, 2021, doi: 10.3390/en14061585.

[4] M. I. Hossain, M. S. Hossain, H. Rahman, E. Nisa, and M. H. Hossain, "A Review on Performance Evaluation of Multilevel Multifunctional Grid Connected Inverter Topologies and Control Strategies Used in PV Systems," www.icrrd.com Qual. Index Res. J., vol. 2, no. 1, pp. 160–188, 2021, doi: 10.53272/icrrd.

[5] Z. Ben Mahmoud and A. Khedher, "A Comprehensive Review on Space Vector Based-PWM Techniques for Common Mode Voltage Mitigation in Photovoltaic Multi-Level Inverters," Energies, vol. 17, no. 4, 2024, doi: 10.3390/en17040916.

[6] R. S. Rani, C. S. Rao, and M. V. Kumar, "a Review of Modulation Schemes for Single Phase Five- Level Cascaded Multilevel Inverter", International Journal of Emerging Technologies and Innovative Research (www.jetir.org), ISSN:2349-5162, vol. 4, no. 11, pp. 453–460, November 2017, doi: Digital Object Identifier/170920, Available: http://www.jetir.org/papers/JETIR1711081.

[7] A. El-hosainy, H. A. Hamed, S. Member, and H. Z. Azazi, "13_A_review_of_multilevel_inverter_topologies, control techniques, and applications," no. December, pp. 19–21, 2017, doi: 10.1109/MEPCON.2017.8301344.

[8] S. R. Hameed and T. H. Al-Mhana, "Cascaded H–Bridge Multilevel Inverter: Review of Topologies and Pulse Width Modulation. Tikrit Journal of Engineering Sciences," Tikrit J. Eng. Sci., vol. 31, no. 1, pp. 138–151, 2024, doi: 10.25130/tjes.31.1.12.

[9] Akshat, M. V. Naik, and R. Kumar, "Performance analysis of an induction motor drive powered by a cascaded H-bridge multilevel inverter," Discov. Electron., vol. 2, no. 1, 2025, doi: 10.1007/s44291-025-00081-y.

[10] B. Jyothi et al., "Evaluation of a multiphase cascaded H-bridge inverter for induction motor operation," Sci. Rep., vol. 14, no. 1, pp. 1–29, 2024, doi: 10.1038/s41598-024-68713-z.

[11] C. W. Winil and V. Aishwarya, "Comparative Study of Reduced Switch Multilevel Inverter Topologies," Lect. Notes Electr. Eng., vol. 1022 LNEE, no. Mli, pp. 461–477, 2023, doi: 10.1007/978-981-99-0915-5_31.

[12] A. Benevieri, S. Cosso, A. Formentini, M. Marchesoni, M. Passalacqua, and L. Vaccaro, "Advances and Perspectives in Multilevel Converters: A Comprehensive Review," Electronics 2024, 13(23), 4736. doi.org/10.3390/electronics13234736.

[13] A. Hren, M. Truntič, and F. Mihalič, "A Survey on the State-of-the-Art and Future Trends of Multilevel Inverters in BEVs," Electron., vol. 12, no. 13, 2023, doi: 10.3390/electronics12132993.

[14] B. Sharma, S. Manna, V. Saxena, P. K. Raghuvanshi, M. H. Alsharif, and M. K. Kim, "A comprehensive review of multi-level inverters, modulation, and control for grid-interfaced solar PV systems," Sci. Rep., vol. 15, no. 1, pp. 1–23, 2025, doi: 10.1038/s41598-024-84296-1.

[15] S. Rathore, M. Kumar Kirar, and S. K. Bharadwaj, "A Review of Cascaded H-Bridge Multilevel Inverter: Control Techniques and its application," Int. Res. J. Eng. Technol., vol. 2, no. 4, pp. 1315–1320, 2015, ISSN: 2395 -0056, Available: http:// www.irjet.net.

[16] M. T. Yaqoob, M. K. Rahmat, S. M. M. Maharum, and M. M. Su'ud, "A review on harmonics elimination in real time for cascaded h-bridge multilevel inverter using particle swarm optimization," Int. J. Power Electron. Drive Syst., vol. 12, no. 1, pp. 228–240, 2021, doi: 10.11591/ijpeds. v12.i1. pp228-240.

[17] A. Bughneda, M. Salem, A. Richelli, D. Ishak, and S. Alatai, "Review of multilevel inverters for PV energy system applications," Energies, vol. 14, no. 6, pp. 1–23, 2021, doi: 10.3390/en14061585.

[18] R. A. Rana, S. A. Patel, A. Muthusamy, C. W. Lee, and H. J. Kim, Review of multilevel voltage source inverter topologies and analysis of harmonics distortions in FC-MLI, vol. 8, no. 11. 2019. doi: 10.3390/electronics8111329.

[19] B. Mosepele, R. Samikannu, and L. Amuhaya, "A structural review on reduced switch count and hybrid multilevel inverters," Front. Energy Res., vol. 12, no. July, 2024, doi: 10.3389/fenrg.2024.1396149.

[20] M. Salem, A. Richelli, K. Yahya, M. N. Hamidi, T. Ang, and I. Alhamrouni, " A Comprehensive Review on Multilevel Inverters for Grid-Tied System Applications", Energies 2022, 15, 6315, pp. 29 August 2022, doi: 10.3390/en15176315.

[21] S. B G, C. Srikanth, and V. Yatnalli, "Review on Multi Level Inverter Topologies and Control Strategies for Solar Power Conversion," Emit. Int. J. Eng. Technol., vol. 8, no. 2, pp. 295–315, 2020, doi: 10.24003/emitter. v8i2.500.

[22] S. Raj and R. Kumar, "A NOVEL CASCADED H-BRIDGE MULTILEVEL INVERTER FOR SOLAR ENERGY INTEGRATION", vol. 7, no., pp. 1831-1841 May, 2022, doi: 10.12732/ijpam. v117i10.22.

[23] D. Mathew and R. C. Naidu, "A review on single-phase boost inverter technology for low power grid integrated solar PV applications," Ain Shams Eng. J., vol. 15, no. 2, p. 102365, 2024, doi: 10.1016/j.asej.2023.102365.

[24] N. G and D. S. D. Torvi, "Multilevel Inverter for Solar Photovoltaic Applications - A Review," Int. J. Res. Appl. Sci. Eng. Technol., vol. 11, no. 7, pp. 439–441, 2023, doi: 10.22214/ijraset.2023.54669.

[25] S. Senthilkumar et al., "a Review on Mppt Algorithms for Solar Pv Systems," Int. J. Res. -GRANTHAALAYAH, vol. 11, no. 3, pp. 25–64, 2023, doi: 10.29121/granthaalayah. v11.i3.2023.5086.

[26] A. Choorakuzhiyil, K. Parate, and J. Joshi, "Comparative Study of Maximum Power Point Tracking Techniques for Photovoltaic Systems," 2023 2nd Int. Conf. Innov. Technol. INOCON 2023, vol. 2015, no. i, 2023, doi: 10.1109/INOCON57975.2023.10100994.

[27] M. L. Katche, A. B. Makokha, S. O. Zachary, and M. S. Adaramola, "A Comprehensive Review of Maximum Power Point Tracking (MPPT) Techniques Used in Solar PV Systems," Energies, vol. 16, no. 5, 2023, doi: 10.3390/en16052206.

[28] M. Madhavan, C. Nallaperumal, and A. Hosseinpour, "Comparison of space vector and switching frequency optimal pulse width modulation for diode free F-type multi level inverter," IET Power Electron., vol. 17, no. 15, pp. 2486–2497, 2024, doi: 10.1049/pel2.12795.

[29] M. Moranchel, F. Huerta, I. Sanz, E. Bueno, and F. J. Rodríguez, "A comparison of modulation techniques for modular multilevel converters," Energies, vol. 9, no. 12, 2016, doi: 10.3390/en9121091.

[30] M. Kurtoğlu and A. M. Vural, "A Novel Nearest Level Modulation Method with Increased Output Voltage Quality for Modular Multilevel Converter Topology," Int. Trans. Electr. Energy Syst., vol. 2022, pp. 1–17, 2022, doi: 10.1155/2022/2169357.

[31] E. B. A. Shah, M. H. Baloch, D. A. M. Soomro, E. S. H. Memon, and D. D. M. Soomro, "Analysis of Harmonic Distortion Reduction through Modular Multi-Level Inverter using Nearest Level Modulation (NLM) Control Strategy," Sukkur IBA J. Emerg. Technol., vol. 4, no. 1, pp. 67–79, 2021, doi: 10.30537/sjet. v4i1.858.

[32] A. Srivastava, A. Chauhan, and A. Tripathi, "Performance Comparison of Asymmetrical Multilevel Inverter with Different Switching Techniques," Energies, vol. 18, no. 3, 2025, doi: 10.3390/en18030715.

[33] E. Hassan Elmabrouk Aboadla, T. Majdee, Khairil A. Bin Aznan, Ashraf Khalil, Sheroz Khan, Mohamed H. Habaebi, Teddy Gunawan, Belal A. Hamidah, Mashkuri Bin Yaacob, "Journal of Electrical Power and Electronics Systems A Comparative Study of Total Harmonics Distortion between Spwm and She-Pwm Modulation Techniques for Inverters," J. Electr. Power Electron. Syst., vol. 1, no. 1, pp. 1–5, 2019, [Online]. Available: www.fazpublishing.com/jepes, doi: 10.1109/ICETSS.2017.8324191.

[34] J. Kulkarni, S. K. Yadav, B. Singh, and N. Kumar, "Power quality investigation of CHB nine-level converter based large-scale solar PV system with different modulation schemes," Energy Convers. Econ., vol. 2, no. 3, pp. 145–156, 2021, doi: 10.1049/enc2.12041.

[35] Micohuang, "Multi-Level Inverters: A Comparative guide to NPC, FCI, and CHB topologies," 27 July 2025a. [Online]. Available: https://www.shunlongwei.com/multi-level-inverters-a-comparative-guide-to-npc-fci-and-chb-topologies/.

